

This manuscript is a **preprint** and has been submitted for possible publication in *Remote Sensing of Environment*. This **has not been peer reviewed before** and is **currently undergoing peer review for the first time**. Please note that subsequent versions of this manuscript may have slightly different content based on reviewer comments. However, if accepted, the final version of this manuscript will be available via the 'Peer-reviewed Publication DOI' link on this webpage. Please feel free to reach out to the authors with suggestions/constructive feedback.

1  
2  
3  
4  
5  
6  
7  
8  
9  
10  
11  
12  
13  
14  
15  
16  
17  
18  
19  
20  
21  
22  
23  
24  
25  
26

### **A Review of Satellite Remote Sensing Techniques of River Delta Morphology Change**

*Dinuke Munasinghe<sup>1\*</sup>, Sagy Cohen<sup>1</sup> and Krishna Gadiraju<sup>2</sup>*

*<sup>1</sup>Department of Geography, University of Alabama, Tuscaloosa, AL, USA.*

*<sup>2</sup>Department of Computer Science, North Carolina State University, Raleigh, NC, USA.*

*\*Corresponding Author: [dsmunasinghe@crimson.ua.edu](mailto:dsmunasinghe@crimson.ua.edu)*

*Table of Contents*

27

28

29 1. Introduction \_\_\_\_\_ 6

30 1.1 The River Delta and its Importance \_\_\_\_\_ 6

31 1.2 The Morphology of a Delta \_\_\_\_\_ 6

32 1.3 Importance of Delta Morphology Change Studies \_\_\_\_\_ 7

33 1.4 Satellite Remote Sensing of Deltaic Morphology Dynamics \_\_\_\_\_ 8

34 1.5 Motivation for this Review \_\_\_\_\_ 9

35 2. Indicators of Delta Morphology Change \_\_\_\_\_ 10

36 3. Delta Shoreline Change Detection Techniques \_\_\_\_\_ 14

37 3.1 Classification Techniques used in Two-Step Change Detection \_\_\_\_\_ 21

38 3.1 (A) Pixel-Based Methods \_\_\_\_\_ 21

39 3.1.1 Manual Digitization \_\_\_\_\_ 21

40 3.1.2 Density Slicing \_\_\_\_\_ 22

41 3.1.3 Image Segmentation and Edge Detection \_\_\_\_\_ 23

42 3.1.4 Band Ratioing \_\_\_\_\_ 24

43 3.1.5 Unsupervised Classification \_\_\_\_\_ 25

44 3.1.6 Supervised Classification \_\_\_\_\_ 26

45 3.1.7 Transformation methods \_\_\_\_\_ 27

46 3.1.8 Artificial Neural Networks (ANN) \_\_\_\_\_ 29

47 3.1.9 Decision Trees and Random Forest Classifiers \_\_\_\_\_ 31

48 3.1.10 Bayesian Networks \_\_\_\_\_ 33

49 3.1.11 Support Vector Machines \_\_\_\_\_ 35

50 3.1.12 Object-based Image Analysis (OBIA) \_\_\_\_\_ 36

51 3.1 (B) Sub-pixel-based methods \_\_\_\_\_ 38

52 3.1.13 Fuzzy Logic \_\_\_\_\_ 39

53 3.1.14 Spectral Mixture Analysis \_\_\_\_\_ 40

54 3.1.15 Sub-Pixel Analysis \_\_\_\_\_ 41

55 3.1.16 General Concerns about Techniques used in Two-Step Change Detection \_\_\_\_\_ 41

56 3.2 Classification Techniques used in One-Step Change Detection \_\_\_\_\_ 42

57 3.2.1 Image Differencing/Layer Arithmetic \_\_\_\_\_ 42

58 3.2.2 Change Vector Analysis \_\_\_\_\_ 43

59 3.3 Ensemble Classifications \_\_\_\_\_ 44

60 4. Other Delta Morphology Change Indicators \_\_\_\_\_ 46

61 4.1 Meander Belts \_\_\_\_\_ 47

62 4.2 Crevasse Splays, Channel Avulsions and Distributary Networks \_\_\_\_\_ 48

63	4.3	Barrier Islands, Beach Spits, and Mouth Bars _____	49
64	5.	Synthesis and Applications _____	51
65	5.1	Machine Learning _____	51
66	5.2	Radar Imagery _____	54
67	6.	Intercomparison of Delta Morphology Feature Extraction Techniques _____	55
68	7.	Future Directions _____	60
69		Direction 1: Utilization of higher resolution imagery and developing better sub-pixel data	
70		mining techniques _____	60
71		Direction 2: Use of automated pattern recognition techniques, universal applicability and	
72		algorithm transferability across platforms _____	63
73		Direction 3: Improvement of Ancillary data _____	64
74		Direction 4: A Global Information System of deltaic data _____	65
75	8.	Conclusions _____	66
76	9.	References _____	67

77  
78  
79  
80  
81  
82  
83  
84  
85  
86  
87  
88  
89  
90  
91  
92  
93  
94

95

## Abstract

96 River deltas are important coastal depositional systems that are home to almost half a billion  
97 people worldwide. Understanding morphology changes in deltas is important in identifying  
98 vulnerabilities to natural disasters and improving sustainable planning and management. Satellite  
99 remote sensing has shown to be a useful technology for analyzing these morphology changes  
100 owing largely to its capability to provide spatially continuous observations. In this paper, we  
101 critically review the literature about satellite remote sensing techniques that were used to study  
102 delta morphology changes.

103 We identify and categorize the techniques reported in the literature into 3 major classes: 1) One-  
104 step change detection, 2) Two-step change detection, and 3) Ensemble Classifications. In total  
105 we offer a review of 18 techniques within these categories. Example studies, the strengths and  
106 caveats in relation to the deltaic environment are discussed for each technique. Our synthesis of  
107 the literature reveals that sub-pixel-based algorithms perform better than pixel-based ones.  
108 Machine learning techniques rank second to sub-pixel techniques although an ensemble of  
109 techniques can be used just as effectively to achieve high feature detection accuracies.

110 We evaluate the 7 most commonly used techniques in literature (Conventional Techniques: (1)  
111 Modified Normalized Difference Water Index (MNDWI), 2) Normalized Difference Water  
112 Index (NDWI), 3) PCA analysis, 4) Unsupervised Classification, and 5) Supervised  
113 Classification)]. Machine Learning techniques: 6) Random Forest Classifier, and 7) Support  
114 Vector Machine) on a sample of global deltas, for delta morphological feature extraction  
115 performance. Findings show the Unsupervised Classification significantly outperforms the others  
116 and is recommended as a first order feature extraction technique in previously unknown, or, data  
117 sparse deltaic territories.

118 We propose four pathways for future advancement in satellite remote sensing of delta  
119 morphology: 1) utilizing new high-resolution imagery and development of more efficient data  
120 mining techniques, 2) moving toward universal applicability of algorithms and their  
121 transferability across satellite platforms, 3) improvement of the availability and use of ancillary  
122 data in image processing algorithms, and 4) development of a global-scale repository of deltaic  
123 data for the sharing of scientific knowledge across regions and disciplines.

124

125

126

127

128

129

130

131

132

133

134

135

136

## 137 **1. Introduction**

### 138 **1.1 The River Delta and its Importance**

139 A river delta is defined as a discrete shoreline protuberance formed from deposition of sediment  
140 where rivers enter oceans, semi enclosed seas (coastal embayments), lakes or lagoons (adapted  
141 from Elliott, 1986). Deltaic regions are home to more than 490 million people, including several  
142 megacities (Syvitski & Saito, 2007). These hubs act as major centers for agriculture (Syvitski &  
143 Saito, 2007), fisheries (Woodroffe *et al.*, 2006), and hydrocarbon production (Syvitski *et al.*,  
144 2009), offering employment opportunities for millions, and consequently making deltaic regions  
145 some of the most economically productive systems in the world (Woodroffe *et al.*, 2006). The  
146 ecological significance of river deltas lies in the fact that they act as coastal storm surge  
147 protectors, biodiversity hotspots, provide habitats for many animal and plant species, provide  
148 pathways for migratory species and carry with them a cultural heritage which is a high revenue  
149 generation mechanism for local communities (Hutchings & Campbell, 2005; Lentz *et al.*, 2016).

### 150 **1.2 The Morphology of a Delta**

151 Morphology, in the simplest of terms, is the configuration or form of a river delta in its natural  
152 environment. The morphology of modern deltaic systems (so named because their  
153 formation/progradation began during the late Holocene period, subsequent to the last glacial  
154 period; Allison *et al.*, 2003) is controlled by the complex interaction between boundary  
155 conditions and forcing factors (Coleman and Wright, 1975; Orton and Reading, 1993; Postma,  
156 1995; Syvitski and Saito, 2007). These forcing factors include (1) supply of bedload and  
157 suspended sediment load: reflecting drainage basin characteristics, water discharge, sediment  
158 yield and grain size; (2) deposition/accommodation space: reflecting sea-level fluctuations,

159 offshore bathymetry, tectonics, subsidence, compaction, and isostasy; (3) coastal energy:  
160 reflecting waves and tides, longshore and cross-shelf transport; and (4) density differences  
161 between effluent and receiving waters defining the dynamics of sediment plumes. The complex  
162 interaction between these factors result in the formation of different features (e.g. main delta  
163 landmass governed by the delta shoreline, sandbars/barrier islands, beach spits). These features,  
164 which are component environments of the delta, collectively describe the morphology of the  
165 delta, reflect the status quo of the river delta, and can be used to monitor changes to the delta  
166 through time.

### 167 **1.3 Importance of Delta Morphology Change Studies**

168 Most modern deltas serve societal needs such as protecting residents, resources, and  
169 infrastructure, or preserving biodiversity and ecosystem services. Human settlements and  
170 infrastructure in low-lying deltaic regions are particularly vulnerable to floods induced by intense  
171 precipitation and storm surges (Motsholapheko *et al.*, 2011; Sanchez-Arcilla *et al.*, 2012). Floods  
172 disrupt cultivation in delta plains, livestock farming, destroy property leading to displacement of  
173 households, interrupt water reticulation systems, and curtail transport systems, thereby impacting  
174 a country's economic growth significantly (Bendsen and Meyer, 2002; Motsholapheko *et al.*,  
175 2011). Therefore, knowledge on morphology change is important to plan engineering works such  
176 as identification of vulnerable areas, installation of coastal defense structures (e.g. breakwaters,  
177 weirs), confinement or widening of river channels, dredging, sand extraction, dam construction,  
178 development of setback planning and hazard zoning.

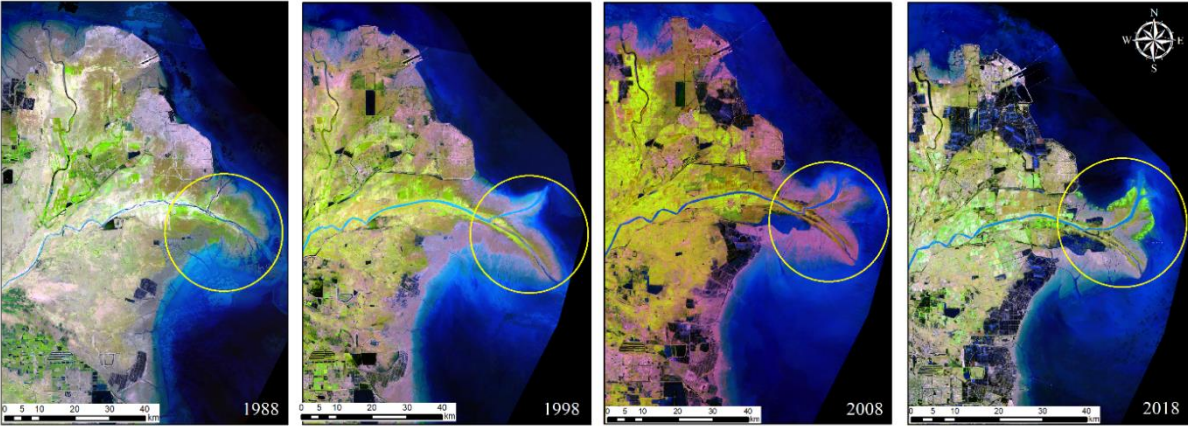
179 In addition to mitigate against flooding, delta morphology change information is also important  
180 for constructing engineering structures for transport, land reclamation and urbanization, erosion-

181 accretion studies, regional sediment budgets, restoration activities for extensively altered deltas,  
182 and for conceptual or predictive modeling of coastal morphodynamics (Sherman and Bauer,  
183 1993, Al Bakri, 1996, Zuzek *et al.*, 2003; see Maiti and Bhattacharya (2009); Masria *et al.*, 2015;  
184 Le *et al.*, 2007). Therefore, understanding and predicting these morphology change dynamics is  
185 of utmost importance for sustainable planning of deltaic communities.

#### 186 **1.4 Satellite Remote Sensing of Deltaic Morphology Dynamics**

187 During the past four decades satellite remote sensing technologies have emerged as a viable  
188 alternative to in-situ observations of river deltas and associated deltaplain morphology changes  
189 (Figure 1: evolution of the Yellow river delta during the satellite era). This is mainly attributed to  
190 their availability over large geographical regions, the effectiveness of the delta-change mapping  
191 techniques, the temporal coverage of a given location, and the relatively low cost for large aerial  
192 extents (Mathers and Zalasiewicz, 1999; Zhao *et al.*, 2008; Zhang *et al.*, 2015; Munasinghe *et*  
193 *al.*, 2018). Although delta morphology mapping based on ground surveys and aerial observations  
194 (e.g. aerial photography, drone footage) is a viable and useful option, such methods are time-  
195 consuming, expensive and, in most cases, cannot provide data on time scales commensurate with  
196 delta morphology change. Remotely sensed data can be seamlessly used as a stand-alone tool, or  
197 in tandem with complementary numerical modeling and statistical efforts.





198 **Figure 1: Landsat satellite imagery showing the evolution of the Yellow River Delta, China from**  
199 **1988 to 2018. The circled area shows the downward development of the Qingshuigou Lobe, and the**  
200 **more prominent upward development of the Qing8 Lobe of the delta.**

### 201 **1.5 Motivation for this Review**

202 The impetus for this review comes from the non-availability of a single robust document in the  
203 literature which portrays past and current research efforts in identifying river delta morphology  
204 changes using satellite remote sensing techniques. The need for such a summation stems from  
205 several reasons. Morphology detection techniques that work well for one particular river delta  
206 might not be ideal for another: This could be due to complications of geometries of river deltas  
207 (e.g. influenced by islands, sandbars), sediment plumes transported by rivers (gradational  
208 deposition at the river mouth) making the identification of the delta boundaries difficult,  
209 geographical location of river delta (governs the type and density of vegetation that grows at the  
210 land-sea margin), and tidal forces (determines formation of islands close to the main delta body  
211 due to breakage) which all act in varying degrees in determining the performance accuracy of  
212 algorithms. This has led to morphology detection algorithms to mostly be location specific. A  
213 summation of knowledge as such also aids in morphology detection algorithm selection and  
214 application to lesser studied deltaic systems globally, done informatively. The transfer of

215 knowledge from prior use cases could be done optimistically (by relative comparison of similar  
216 delta forms and geographical regions) and with caution (prior understanding of limitations of  
217 detection algorithms). Thus, for current research frontiers in deltaic research to expand, a need  
218 arises for a comprehensive, organized summary of historical and emerging techniques of delta  
219 change mapping of key deltaic environments.

220 We also perform a comparison of remote sensing techniques on an array of delta types (river-,  
221 tide-, wave-dominated) from a global sample of deltas to understand the performance of  
222 techniques under varying fluvial and marine conditions. Elucidating which technique(s) work  
223 best in delta morphological feature extraction would allow us to infer why particular techniques  
224 underperform in different regions of the world. This will also highlight some of the inherent  
225 problems of particular techniques and will offer a pathway for improving existing algorithms and  
226 development of new ones to monitor river delta morphological change.

227 This document reviews the content of 146 articles/book chapters which used remote sensing  
228 technologies to detect deltaic features and their changes, and a further 38 articles/book chapters  
229 to gather supplementary information on river delta research and technological advances in  
230 computational algorithm development. Every effort has been taken to cover the breadth of  
231 remote sensing techniques that were used in delta morphology research from 1980 until present  
232 day.

## 233 **2. Indicators of Delta Morphology Change**

234 A river delta is a collection of different component environments (as described in section 1.2).  
235 Changes to these components result in the changes in geometries, sediment facies and  
236 depositional architecture of the delta. Thus, these components can be used as ‘indicators’ to

237 assess changes to the morphology and can be quantitatively used to derive delta evolution. For  
238 example, a decrease in sediment fluxes to the delta can move it from a condition of active growth  
239 to a destructive phase portrayed by the recession of the land-sea margin (i.e. the delta shoreline).  
240 In a second example, strong wave climates effectively diffuse fluvial sediment, thereby limiting  
241 mouth bar growth and make the delta mainland more erosion prone, and vice versa. Therefore,  
242 as per the above two examples, the delta shoreline and presence/absence of mouth bars can be  
243 used as indicators to assess changes to river delta morphology.

244 Although there exist a plethora of morphology change indicators, it has to be noted that the focus  
245 of this review will only be on, a) indicators that can be identified using satellite remote sensing  
246 (e.g. shelf depth, (water depth reached by the submerged delta), although a factor governing delta  
247 morphology, cannot be assessed using satellite remote sensing), and b) indicators that directly  
248 reflect morphology-change of a delta (e.g. indicators reflecting changes to the effective deltaic  
249 landmass (i.e. the shoreline)) as opposed to indicators of forcing factors which act as causal  
250 factors of morphology change (e.g. drainage basin-averaged climate, which in turn can have an  
251 effect on erosion of delta plain and sediment loading into feeder river).

252 Based on above selection criteria, we categorize all satellite-detectable indicators which reflect  
253 morphology change into 5 classes summarized from studies conducted by Syvitski and Saito  
254 (2007), Mathers and Zalasiewicz, (1999), Ulrich *et al.* (2009), Passalacqua, (2017). Table 1  
255 provides an overview of these indicators, and the role they play in structuring the overall  
256 morphology of the delta.

257

258 **Table 1: Change indicators and their representation of delta morphology**

This manuscript is a **preprint** and has been submitted for possible publication in *Remote Sensing of Environment*. This **has not been peer reviewed before** and is **currently undergoing peer review for the first time**. Please note that subsequent versions of this manuscript may have slightly different content based on reviewer comments. However, if accepted, the final version of this manuscript will be available via the ‘Peer-reviewed Publication DOI’ link on this webpage. Please feel free to reach out to the authors with suggestions/constructive feedback.

Class	Indicator	Role of Indicator in Delta Morphology Change Representation	Can be Remotely Sensed? (Y/N)	Included in Review? (Y/N)
1	Shoreline	Governs the land-sea margin, determines the effective landmass available for human consumption, and determines subaerial view (plan view) of the delta.	Y	Y
2	Crevasse Splays and Channel Avulsions	Channel avulsions in deltaic areas start with the formation of a crevasse splay. Crevasse splays (deposits of sediment in the shape of a fan or lobe formed by river channels as a result of point failures of a levee) help better understand how rivers naturally distribute water and sediment across floodplains, local rates of sediment accumulation and sediment delivery to coastal regions, and influences on floodplain topography and alluvial architecture, and help make informed decisions on land-management solutions such as engineered diversions (Nienhuis et al., 2018).	Y	Y
3	Number and Size of Distributary Channels, and Meander belts	Avulsions and other channels on the delta make up the distributary network. Proper understanding of the size of the distributary channels and the ways in which they migrate through time is critical to many geomorphological and river management problems on a delta (Seker et al., 2005; Yang et al., 1999). Channel erosion and bank failure cause obstruction of navigation routes, changes to channel geomorphology, and most importantly changes to flood levels which can have adverse impacts on the infrastructure of the delta plain.	Y	Y
4	Barrier Islands, Beach Spits, and Mouth Bars	These are deltaic features that result from the dynamic interaction of fluvial sediment supply and the redistribution of sediment by marine processes at the river mouth-sea interface. Rapid deposition on river-mouth bars can cause their seaward progradation, which, through the control of upstream siltation in the main river channel, can serve as a stimulus to river channel migration. Heavy	Y	Y

		sedimentation in the lower reaches of the river channel can also cause the riverbed to aggrade and increases the flood risk on the floodplain, making the river channel avulsion-prone. Beach spits and barrier islands function more in the capacity of coastal storm surge attenuation and wave and tidal erosion control which impact the shoreface.		
5	Gradient of Delta Plain	Measured from the apex of the delta to the coast along the main channel (Syvitski and Saito, 2007), the gradient of the delta plain is a vertical measure of morphology. This in addition to the sediment supply to sediment retention on the delta plain, can be significantly impacted by subsidence of the delta plain itself. Subsidence related morphological changes to the gradient might not be reflected by the land-sea boundary but can be reflective in flood extents during extreme events which impact floodplain architecture.	Y	*N

259

260 \* studies pertaining to the gradient of the delta plain will not be discussed in this review for two reasons. Firstly, the majority of the studies related to the gradient  
261 in the literature are from a geological perspective without any substantial remote sensing component to them. Thus, they do not scope well within the constraints  
262 of this review. Secondly, even the studies that did discuss remotely sensed changes in river delta gradient, were done so as secondary derivatives of changes in  
263 land subsidence of the delta. Subsidence mapping is an entirely vast and different field of remote sensing which would constitute a separate review of its own.

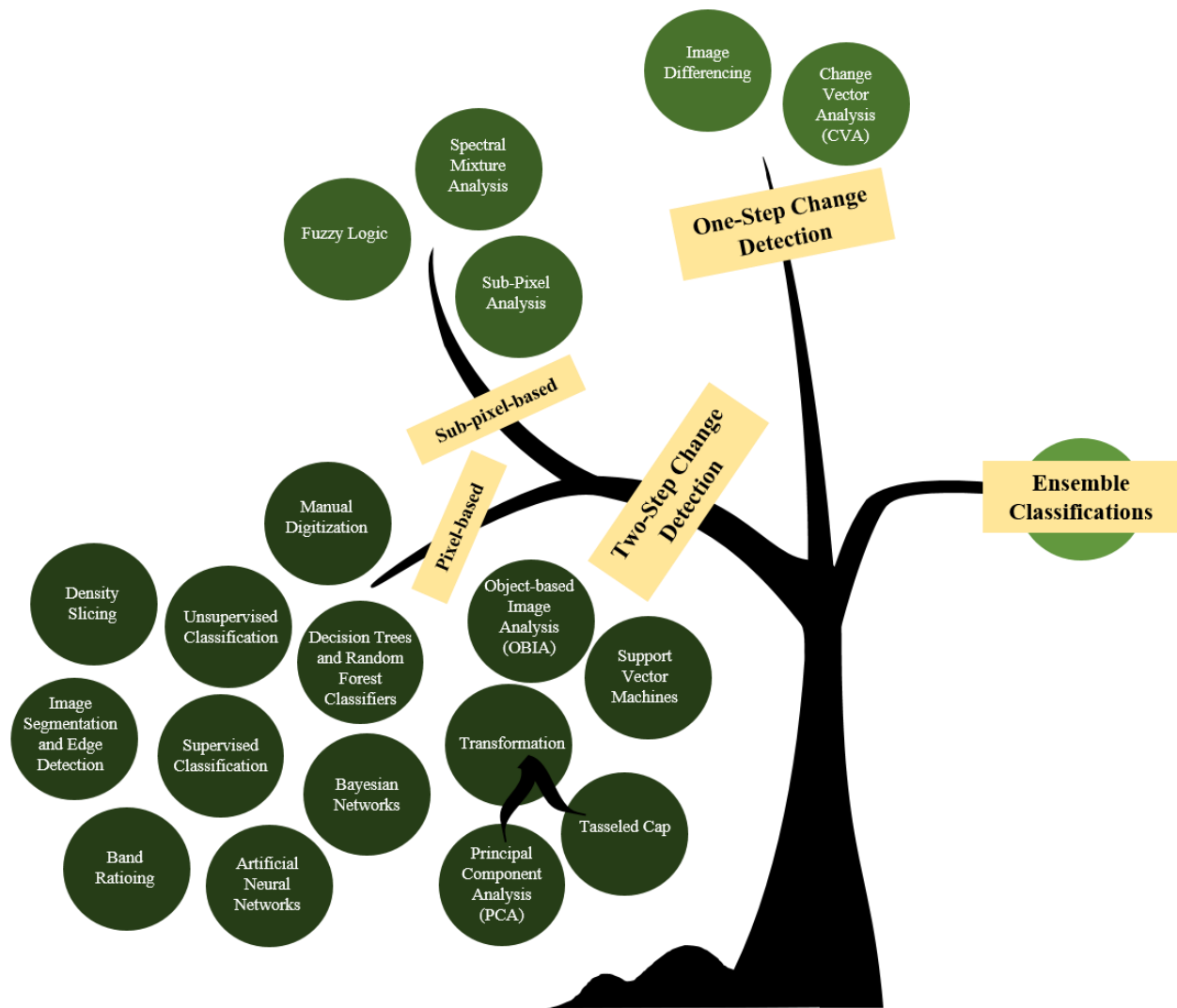
264 The change in deltaic shoreline can be regarded as the most important environmental descriptor  
265 of delta morphology, as it is the only parameter that reflects the ‘quantity’ of landmass available  
266 for human consumption indicating how the delta front prograded or degraded over the years. In  
267 comparison, other indicators detect morphology changes ‘on’ the deltaic landmass and thus has  
268 garnered a lesser importance in literature (over 90% of the studies reviewed for morphology  
269 change were based on the shoreline). Delta shoreline changes are described in section 3, and  
270 studies discussing all other indicators are summarized in section 4.

### 271 **3. Delta Shoreline Change Detection Techniques**

272 Delta progradation/degradation determination through remote sensing relies on the varied  
273 spectral response of the land-water boundary (i.e. the shoreline) at different wavelengths.  
274 Different landforms produce characteristic surface spectral responses as products of the  
275 combination of the terrain color and surface moisture linked with composite materials, texture  
276 and structure properties of the exposed portions, terrain geometry and land cover. A large  
277 number of techniques for delta progradation detection from satellite imagery have been  
278 developed over the years and can be classified into three broad categories of change detection  
279 methods (Figure 2): 1) Two-step Change Detection: use of a remote sensing technique(s) to  
280 delineate morphology for a particular time step, use the same or different set of technique(s) to  
281 retrieve morphology at a different time step and compare between them; 15 such techniques will  
282 be discussed, 2) One-step change detection: The use of a remote sensing technique(s) on  
283 multirate imagery to detect change in one step; two such techniques will be discussed: a) Layer  
284 Arithmetic: use of band mathematics on the reflectance values to compare between multi-date  
285 imagery, b) Change Vector Analysis: use of the radiometric properties of multi-date imagery to

286 yield both magnitude and direction of change, and 3) Ensemble Classification: use of a mixed  
287 methods approach.

288 It is important to note, and user applications need to pay attention to the fact that, the location of  
289 a shoreline on a satellite image might not be the topographical boundary between land and water  
290 as it is an instantaneous one influenced by seawater level fluctuations caused by waves, tides and  
291 local seasonal sea level changes. Therefore, it would be erroneous to apply said shoreline  
292 detection techniques to a single image representative of a time step, as these external forces can  
293 substantially affect water levels (Walker and Hammack, 2000) and consequently the boundary,  
294 without necessarily indicating a morphological change. There are statistical methods to correct  
295 for the shoreline position (Zhang *et al.*, 2018) if changes of shorter time steps are desired (e.g.  
296 change every year during a 5-year period). For longer time scale analysis (e.g. change every 5  
297 years for a 30-year period), a composite, representative of the deltaic region, using imagery over  
298 a few consecutive months (e.g. 6 months), is created, and the averaged raster is used as a single  
299 time step.



300

301 **Figure 2: Classification of remote sensing techniques used for river delta morphology change**  
 302 **detection**

303 The discussion of each technique is framed on the conceptual background of the technique, how  
 304 and why it is applied to deltaic feature detection, the technical merit of application, and its  
 305 caveats informed by the conclusions and recommendations of the literature reviewed. We present  
 306 a summary of all techniques reviewed in this paper along with example studies in Table 2 below  
 307 for the readership to revert to, during the length of the document, as a quick reference guide.



**Table 2: A summary of remote sensing techniques of river delta morphology change identification**

<b>Technique</b>	<b>Example Studies</b>	<b>River Delta (Country)</b>	<b>Satellite Platform</b>
Manual Digitization	Yang (1996)	Yellow (China)	Landsat MSS, Landsat TM
	Yang <i>et al.</i> (1999)	Yellow (China)	Landsat MSS, Landsat TM
	Chu <i>et al.</i> (2006)	Yellow (China)	Landsat MSS, Landsat TM
	Zhao <i>et al.</i> (2008)	Yangtze (China)	Landsat TM, Landsat ETM+
	Marghany <i>et al.</i> (2010)	Kuala Terengganu (Malaysia)	ERS-1, RADARSAT-1
	El Asmar and Hereher (2011)	Nile (Egypt)	Landsat MSS, Landsat TM, SPOT-4
	Kuenzer <i>et al.</i> (2014)	Yellow (China)	Landsat MSS, Landsat TM
	Duțu <i>et al.</i> (2014)	Danube (Romania/Ukraine)	Landsat TM, Landsat ETM+
	Ahmed <i>et al.</i> (2018)	Ganges-Brahmaputra-Meghna (India)	Landsat TM, Landsat ETM+
Density Slicing	Mouchot <i>et al.</i> (1991)	Mackenzie (Canada)	Landsat TM
	Mathers and Zalasiewicz (1999)	Red (Vietnam)	Landsat TM
	Ryu <i>et al.</i> (2002)	Gosmo Bay (Korea)	Landsat TM, ASTER
	Maiti and Bhattacharya (2009)	Subarnarekha and Rasulpur (India)	Landsat MSS, Landsat TM, Landsat ETM+, ASTER
	Mallinis <i>et al.</i> (2011)	Nestos (Greece)	Quickbird
	Allen <i>et al.</i> (2012)	Wax Lake (USA)	Landsat TM, Landsat ETM+
	Kong <i>et al.</i> (2015)	Yellow (China)	Landsat MSS, Landsat TM, Landsat ETM+
	Ghoneim <i>et al.</i> (2015)	Nile (Egypt)	Landsat MSS, Landsat TM, Landsat ETM+
	Dada <i>et al.</i> (2018)	Niger (Nigeria)	Landsat TM, Landsat ETM+
Image Segmentation and Edge Detection	Lee and Jurkevich (1990)	Chesapeake Bay (USA)	Saesar, Shuttle Imaging Radar (SIR)
	Mason and Davenport (1996)	Wash delta/estuary (UK)	ERS-1
	Niedermeier <i>et al.</i> (2000)	Elbe (Germany)	ERS-1 and ERS-2
	Bayram <i>et al.</i> (2008)	Bhosporous (Turkey)	Corona, IRS-1D, Landsat ETM+
	Al Fugura <i>et al.</i> (2011)	Kuala Terengganu (Malaysia)	RADARSAT-1
Band Ratioing	Yang <i>et al.</i> (1999)	Yellow (China)	Landsat MSS, Landsat TM
	El-Raey <i>et al.</i> (1999)	Nile (Egypt)	Landsat MSS
	Ryu <i>et al.</i> (2002)	Gosmo Bay (Korea)	Landsat TM, ASTER

	<p>Guariglia <i>et al.</i> (2006)  Ekercin (2007)  Kuleli (2010)  Cui and Li (2011)  Mukhopadhyay <i>et al.</i> (2012)  Niya <i>et al.</i> (2013)  Kundu <i>et al.</i> (2014)  Louati <i>et al.</i> (2015)  Nitze and Grosse (2016)  Sun <i>et al.</i> (2018)  Wang <i>et al.</i> (2019)  Da Silva <i>et al.</i> (2019)  Viaña-Borja and Ortega-Sánchez (2019)</p>	<p>Ionian coast (Italy) inclusive of deltas  nothern coast of Turkey including deltas  Cukurova (Turkey)  Yellow (China)  Puri coast and Mahanadi (India)  Dalaki (Iran)  Sagar Island, GBM (India)  Medjerda (Tunisia)  Lena (Russia)  Yangtze (China)  Yellow (China)  Parnaíba (Brazil)  Guadalfeo, Adra, and Ebro (Spain)</p>	<p>Landsat TM, Landsat ETM+, SPOT XS, Corona  Landsat MSS, Landsat TM, Landsat ETM+  Landsat TM  Landsat MSS, Landsat TM, Landsat ETM+  Landsat TM  Landsat TM  Landsat TM, Landsat ETM+, Landsat OLI  Landsat TM, Landsat ETM+, Landsat OLI  Landsat MSS, TM, OLI, GF-1 PMS, SPOT-7  Landsat TM, Landsat OLI  Landsat MSS, TM, ETM+, OLI  Landsat TM, Landsat ETM+, Landsat OLI</p>
Unsupervised Classification	<p>Wilson (1997)  Frihy <i>et al.</i> (1998)  Guariglia <i>et al.</i> (2006)  Ekercin (2007)  Nath and Deb (2010)  Mukhopadhyay <i>et al.</i> (2012)  Muster <i>et al.</i> (2012)  Kundu <i>et al.</i> (2014)  Buono <i>et al.</i> (2017)</p>	<p>Fitzroy (Australia)  Nile (Egypt)  Ionian coast (Italy) inclusive of deltas  nothern coast of Turkey including deltas  Okavango Delta (Botswana)  Puri coast and Mahanadi (India)  Lena (Russia)  Sagar Island of the GBM (India)  Yellow (China)</p>	<p>Corona  Landsat MSS, Landsat TM  Landsat-TM, Landsat ETM+, SPOT-PX/XS, Corona  Landsat MSS, Landsat TM, Landsat ETM+  AVHRR  Landsat TM  Proba -1  Landsat TM  RADARSAT-2</p>
Supervised Classification	<p>Sgavetti and Ferrari (1988)  Ciavola <i>et al.</i> (1999)  Seker <i>et al.</i> (2003)  El-Kawya <i>et al.</i> (2011)  Masria <i>et al.</i> (2015)</p>	<p>Po and Adige (Italy)  Shkumbini, Semani and Vjosë (Albania)  Riva (Turkey)  Nile (Egypt)  Nile (Egypt)</p>	<p>Landsat TM  Landsat TM  Landsat MSS, Landsat TM, Landsat ETM+  Landsat TM, Landsat ETM+  Landsat TM, Landsat ETM+</p>

Transformation Methods Principal Component Analysis (PCA)	El Raey <i>et al.</i> (1995) Li and Yeh (1998) Kushwaha <i>et al.</i> (2000) Seto <i>et al.</i> (2002) Li and Yeh (2004) Ghanavati <i>et al.</i> (2008) Ghoneim <i>et al.</i> (2015)	Nile (Egypt) Pearl (China) West Bengal coast inclusive of deltas (India) Pearl (China) Pearl (China) Hendijan (Iran) Nile (Egypt)	Landsat MSS, Landsat TM Landsat TM ERS-1 Landsat TM Landsat TM Landsat TM, Landsat ETM+ Quickbird, Worldview-2
Tasseled Cap Transformation	Nandi <i>et al.</i> (2016) Chen <i>et al.</i> (2019)	Sagar Island, GBM (India) Yangtze (China)	Landsat MSS, Landsat TM, Landsat ETM+ Landsat OLI
Artificial Neural Networks (ANN)	Berberoglu <i>et al.</i> (2000) Zhu (2001) Del Frate <i>et al.</i> (2012) Ding (2013)	Cukurova (Turkey) Pearl (China) Italian coastline inclusive of deltas Yellow (China)	Landsat TM Landsat MSS, Landsat TM COSMO-SkyMed Landsat TM, Landsat ETM+
Decision Trees and Random Forest Classifiers	Ottinger <i>et al.</i> (2013) Kuenzer <i>et al.</i> (2014) Haas and Bun (2014) Banks <i>et al.</i> (2015) Berhane <i>et al.</i> (2018)	Yellow (China) Niger (Nigeria) Yellow, Pearl (China) Kitikmeot region (Canada) inclusive of deltas Selenga (Russia)	Landsat TM Landsat TM, Landsat ETM+ Landsat TM, HJ-1A/B satellites RADARSAT-2, Landsat TM Worldview-2
Bayesian Networks	Gutierrez <i>et al.</i> (2011) Yates and Cozannet (2012)	U.S. Atlantic Coast inclusive of deltas European coasts inclusive of deltas	Areal observations used as input
Support Vector Machines	Xu <i>et al.</i> (2012) Masria <i>et al.</i> (2015) Petropoulos <i>et al.</i> (2015) Gou <i>et al.</i> (2016)	Yellow (China) Nile (Egypt) Axios and Aliakmonas (Greece) Yellow (China)	RADARSAT-2 Landsat TM, Landsat ETM+ Landsat TM ALOS-2

Object-based Image Analysis	Cao <i>et al.</i> (2007) Liu <i>et al.</i> (2014) Demers <i>et al.</i> (2015) Zhu <i>et al.</i> (2018)	Yellow (China) Yellow (China) Islands of Mackenzie Delta (Canada) Yellow (China)	SPOT 5 Landsat TM, Landsat ETM+, HJ-1A/B satellites RADARSAT-2 Landsat MSS, Landsat TM, Landsat OLI
Fuzzy Logic	Dellepiane <i>et al.</i> (2004) Foody <i>et al.</i> (2005) Ghanavati <i>et al.</i> (2008) Dewi <i>et al.</i> (2016)	coastline in Genova (Italy) inclusive of deltas coast in Terengganu (Malaysia) inclusive of deltas Hendijan (Iran) deltaic region in the Sayung District (Indonesia)	ERS-1, ERS-2 IKONOS Landsat TM, Landsat ETM+ Landsat TM, Landsat ETM+, Landsat OLI
Spectral Mixture Analysis	Liu <i>et al.</i> (2016) Liu <i>et al.</i> (2017)	Yellow (China) Pearl (China)	Landsat OLI Landsat OLI
Sub-Pixel Analysis	Wei <i>et al.</i> (2008)	Yellow (China)	ASTER
Image Differencing	Yeh and Li (1997) Xia (1998) El-Raey <i>et al.</i> (1999) Adegoke (2010)	Pearl (China) Pearl (China) Nile (Egypt) Niger (Nigeria)	Landsat MSS, Landsat TM Landsat TM Landsat MSS Landsat TM, Landsat ETM+
Change Vector Analysis	El-Raey <i>et al.</i> (1999) Seto <i>et al.</i> (2002)	Nile (Egypt) Pearl (China)	Landsat MSS Landsat TM

## 327 **3.1 Classification Techniques used in Two-Step Change Detection**

### 328 **3.1 (A) Pixel-Based Methods**

#### 329 *3.1.1 Manual Digitization*

330 Deltaic coastlines are delineated manually based on the delineator's/digitizer's knowledge of the  
331 morphological features, vegetation and sediment characteristics of the delta. Compared to  
332 computer aided classification techniques, manual operation takes advantage of the judgment  
333 skills and interpretation of humans in defining what and where the boundary is between land and  
334 water.

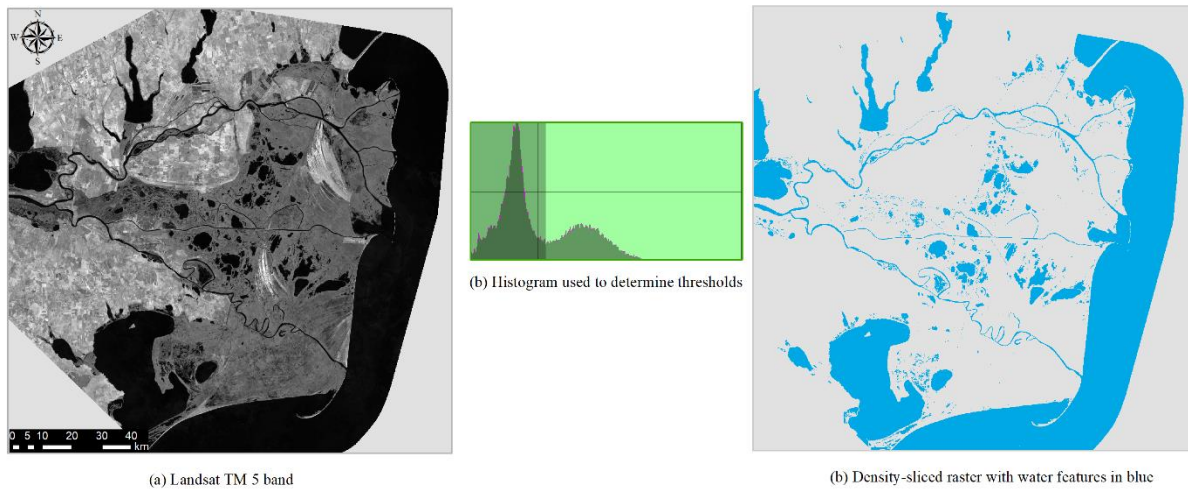
335 The combination of digitization and automatic boundary detection algorithms (discussed later) to  
336 detect the land–ocean shoreline boundaries were proven to be successful (Kong *et al.*, 2015).  
337 However, this technique has several inherent problems. In addition to the inaccuracies induced  
338 through the monotonous nature of digitization, it is also challenging for the human eye to  
339 interpret the boundary (based largely on digitizer's experience) since, mainly in low-resolution  
340 images, color shades may decay gradually (Niedermeier *et al.*, 2005). Presence of water  
341 saturated zones in the vicinity of the land water boundary could complicate the issue. Therefore,  
342 calculations have to be performed in order to recognize if the inaccuracies constitute a significant  
343 source of error in comparison to the magnitude of the overall changes in the delta (Chu *et al.*,  
344 2006). This approach is also highly time-consuming and tedious. It is therefore expensive (labor  
345 cost) and ineffective when a large number of images need to be analyzed.

### 346 3.1.2 Density Slicing

347 The concept of density slicing involves classifying the remotely-sensed image into land and sea,  
348 often by identifying a threshold value for a single spectral band. In order to determine this  
349 critical threshold without bias, a histogram analysis is often performed (Figure 3). Ryu *et al.*  
350 (2002) and Shen *et al.* (2008) showed that in tidal flat zones, thermal-infrared (TIR) band is the  
351 most sensitive to the location of waterline through density slicing. Work on Landsat has shown  
352 that mid-infrared bands (band 5 in the case of Landsat TM) is the most suitable for extracting the  
353 land water interface because it exhibits a strong contrast between land and water features due to  
354 the high degree of absorption of the mid-infrared wavelength by water (Manavalan *et al.*, 1993;  
355 Kelly *et al.*, 1998; Frazier and Page, 2000; Lee *et al.*, 2001; Alesheikh *et al.*, 2007).

356 While overall successful, this method carries with it certain caveats. Although land and water  
357 generally appear to be spectrally separable, the accuracy of waterline prediction is sometimes  
358 low due to the dynamic and complex land-water interactions in coastal deltaic regions. This  
359 could be due to spectral confusion, arising from effects such as variable depth and turbidity,  
360 together with the spatial resolution of the imagery, which influences the clarity of boundaries and  
361 proportion of mixed pixels, limiting the accuracy of shoreline mapping (Frazier and Page, 2000;  
362 Ryu *et al.*, 2002; Malthus and Mumby, 2003). Also, the use of one spectral band usually does not  
363 allow every type of change to be detected (Gong, 1993). Density slicing alone is not sufficient in  
364 determining the shoreline and, therefore, typically used in conjunction with other methods to  
365 obtain higher delta shoreline classification accuracies (Marghany *et al.*, 2010).

366



367

368 **Figure 3: Density Slicing of band 5 (Landsat TM) of the Danube delta region to obtain a land-water**  
369 **raster. The shoreline was subsequently extracted using GIS methods.**

### 370 3.1.3 Image Segmentation and Edge Detection

371 Image segmentation and edge detection algorithms follow the process of manual digitization  
372 more closely by dividing an image into different regions where sharp intensity alterations occur.  
373 The “alternative connective approach”, one of two major image segmentation and edge detection  
374 algorithms is used in deltaic research where it seeks to grow homogeneous regions by merging  
375 pixels or sub-regions on the basis of some similarity criterion (Lemoigne and Tilton, 1995). This  
376 approach is based on ‘guiding’ the remote sensing software by manually identifying points along  
377 the shoreline of the original image. The software then examines the edges of the image following  
378 these points. The parameters by which the shoreline is identified are determined by the analyst.  
379 This heuristic search is found to be faster and more reliable than entirely automated approaches  
380 (Loos and Niemann, 2002) due to the input of previously gathered information by the analyst.

381 Albeit its success, this method also has its limitations in possible inclusion of different earth  
382 feature classes into the same region, making spectral separation and subsequent identification of  
383 thematic information classes difficult. As White and El Asmar (1999) and Heimann *et al.* (2004)  
384 stated, since the classical region growing methods (classifying neighboring pixels outward from  
385 a point of origin based on similarity of reflectance of the originating pixel) yield outcomes in  
386 accordance with the contrast of the image, contrast similarities between land and water zones  
387 impedes the extraction of coastline from other existing constituents and could result in  
388 irregularities of coastline extractions.

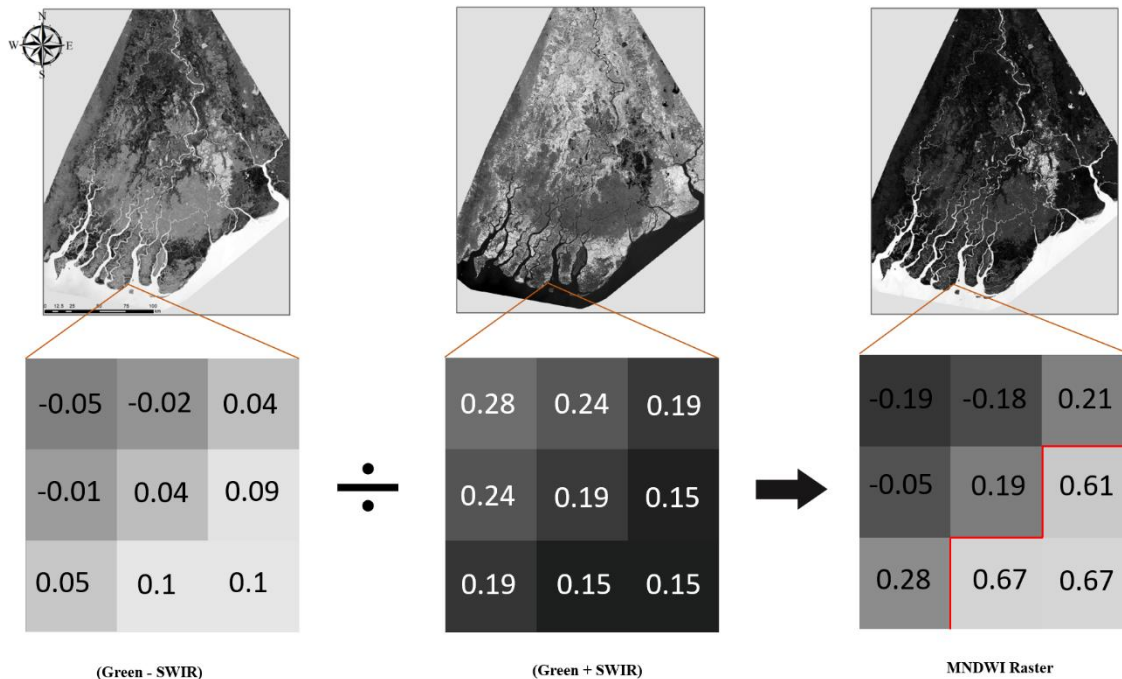
#### 389 3.1.4 Band Ratioing

390 This method exploits the near infrared (NIR) and short-wave infrared (SWIR) bands whose  
391 wavelengths are absorbed by water, resulting in surface water rendered as black color in the  
392 processed image. A combination of these spectral bands ( $(\text{NIR}-\text{SWIR})/(\text{NIR}+\text{SWIR})$ ) is used to  
393 reduce the effect of suspended sediment near shorelines (Lohani & Mason, 1999; Lodhi *et al.*,  
394 1997) and accentuate higher reflectance characteristics from soil and healthy vegetation,  
395 providing a context for the land/water interface (Braud and Feng, 1998; Fraizer and Page, 2000;  
396 Guariglia *et al.*, 2006). In comparison to other methods, ratioing is a relatively rapid means of  
397 identifying areas of change.

398 However, there are certain downsides to this method. The Band 2/Band 5 ration has a value  
399 greater than one for water and less than one for land in large areas of the coastal zone (Alesheikh  
400 *et al.*, 2007). Image processing software use this ratio as an algorithm for separating water from  
401 land from TM or ETM+ imagery. This ratio works well in coastal zones covered by soil, but not  
402 in land with vegetative cover. This can lead to mistakenly classifying other land use types as  
403 water (Alesheikh *et al.*, 2007). Therefore, this is a readily go-to method if the aim is to rapidly



404 extract the coastline. However, if the goal is accurate coastline extraction, then this might not be  
 405 the most suitable. Figure 4 below shows an example application we conducted on the Irrawaddy  
 406 delta in the shoreline extraction process using Landsat-8 imagery.



407 **Figure 4: Band ratioing of Landsat-OLI imagery of the Irrawaddy river delta to produce a land-**  
 408 **water raster after which the shoreline is extracted using GIS methods. The combination and ratio**  
 409 **used here is the Modified Normalized Water Index (MNDWI; Xu, 2006) used to accentuate water**  
 410 **features. *left:* A subtracted difference raster of Band 6 (SWIR) is and Band 3 (Green) is generated**  
 411 **(the blow-up denotes raster values of the selected region). *Middle:* An added difference raster of**  
 412 **Band 6 (SWIR) is and Band 3 (Green) is generated. *Right:* The difference-rasters are ratioed to**  
 413 **produce the MNDWI feature-accentuated raster.**

### 414 3.1.5 Unsupervised Classification

415 Unsupervised classification is an effective method of natural clustering and extracting land-cover  
 416 information of remotely sensed image data based on spectral properties of pixels. Compared to  
 417 supervised classification (discussed in 3.1.6), unsupervised classification requires minimal initial

418 input from the analyst (determining the clustering algorithm and desired number of classes) as it  
419 does not require training data. The clustering process results in a classification map consisting of  
420  $n$  spectral classes. The analyst then attempts to assign or transform the spectral classes into  
421 thematic information classes of interest (e.g., forest, agriculture). Many clustering algorithms  
422 have been developed to date (e.g. ISODATA Clustering, K-Means).

423 Unsupervised methods, although not completely exempt from the user's interaction, require less  
424 inputs than their supervised counterparts and is computationally efficient. However, the user  
425 must have knowledge of the area and understand the spectral characteristics of the terrain in  
426 order to relate the classes to actual land cover types (such as water features, wetlands, developed  
427 areas, coniferous forests, etc.). Difficulties in obtaining consistent classes from images taken at  
428 different times, owing to variability in illumination, atmospheric effects, and instrumental  
429 response, have been reported (Adams *et al.*, 1995). Also, some spectral clusters may be  
430 meaningless because they represent mixed classes of earth surface materials. It has been noted in  
431 the literature that although the use of unsupervised classification is nearly a labor-independent  
432 analysis, this technique does not lead to the most detailed analysis and cannot produce the  
433 highest classification accuracy (Congalton, 1991; Xia, 1998; Enderle and Weih, 2005).

### 434 3.1.6 *Supervised Classification*

435 In Supervised classification, the analyst selects sample pixels in an image that are representative  
436 of land cover classes, and then directs the image processing software to use these end-member  
437 pixels (training pixels) as references for the classification of all other pixels in the image  
438 (determination of maximum likelihood of image pixels of a land use class based on training  
439 data). Training sites are selected based on the analyst's knowledge and experience of image  
440 interpretation. The analyst also designates the number of classes that the image is classified into.

441 Since supervised classification is based on prior knowledge about the land cover and their typical  
442 spectral characteristics by the analyst, this method is deemed one of the more successful methods  
443 of delta morphology detection and is commonly used as a benchmark to test other algorithms  
444 (Khatami *et al.*, 2016). Higher classification accuracies resulting from supervised classification  
445 motivated researchers to combine this technique with other methods. Shalaby and Tateishi  
446 (2007), for example, concluded that the use a combination of supervised classification and visual  
447 interpretation analysis increased the overall classification accuracy by approximately 10%.  
448 However, as the training sites are selected based on the knowledge and experience of the analyst,  
449 there is always the possibility that the sample pixels that one selects for a given information class  
450 (e.g. shoreline) will not be homogenous across the entire study domain (i.e. training areas will  
451 not encompass unique spectral signatures of a particular land feature). In addition, since this is a  
452 user driven method, it can be a time consuming and an exhaustive one, if done for multiple time  
453 steps over different study domains.

### 454 *3.1.7 Transformation methods*

455 When multispectral images are used to detect change of delta morphology, a reduction of the  
456 number of bands is often warranted in order to identify dominant patterns in the imagery (i.e.  
457 enhance the original classification feature space) without compromising the variance. Although  
458 simple band mathematics can be used and is straightforward (e.g. density slicing, band ratioing),  
459 it can be inefficient when the number of spectral bands of the image exceeds three. To overcome  
460 these difficulties the process of image transformation was introduced. Different transformation  
461 methods have been developed over the years, and two of those have been reported in delta  
462 morphological studies: Principal Component Analysis (PCA) and Tasseled Cap Analysis (TCA).

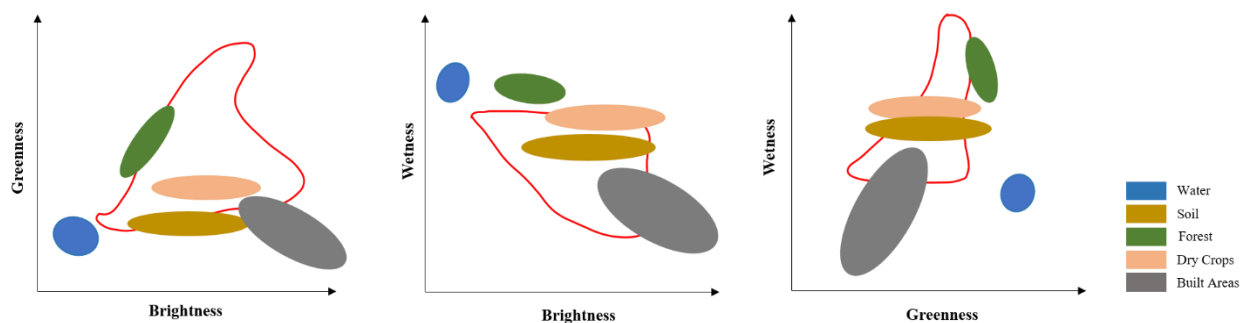
463 The central concept of a PCA is to reduce the dimensionality of a dataset consisting of many  
464 interrelated variables, while retaining as much variation present in the dataset as possible. This is  
465 achieved by transforming the data to a new set of variables (principal components) which are  
466 uncorrelated and ordered so that the first few retain most of the variation present in all the  
467 original variables (Deng *et al.*, 2008). The procedure works as such that subsequent to  
468 performing a PCA on multi temporal imagery, conventional clustering methods (e.g.  
469 unsupervised) can be applied to the first few principal components to produce thematic maps  
470 representative of different earth features. This method was shown to improve accuracy gains  
471 when utilized with other techniques in the image classification process (Khatami *et al.*, 2016).

472 Although comparatively PCA analysis has advantages over simple band mathematics techniques  
473 (i.e. band ratioing, band differencing), it introduces difficulties in interpreting and labeling each  
474 component image (to associate physical scene characteristics with the individual components).  
475 This type of analysis is also scene dependent and is difficult to obtain the ‘from-to change’ class  
476 information (change in pixel information from an earlier time step to a later one) when detecting  
477 change over multiple time steps. Moreover, it was found that the application of PCA for multiple  
478 time step analysis is subject to the condition that the areas of change must be a small proportion  
479 of the entire study area (Gong, 1993; Seto *et al.*, 2002).

480 TCA transformation rotates multispectral data and creates three planes: Brightness (B),  
481 Greenness (G) and Wetness (W) (Crist, 1985). The Brightness band is a weighted sum of all  
482 reflective bands and can be interpreted as the overall brightness or albedo at the earth’s surface.  
483 The Greenness band primarily measures the contrast between the visible bands and near-infrared  
484 bands and is similar to a vegetation index. The wetness band measures the difference between  
485 the weighted sum of the visible and near-infrared bands and the mid-infrared bands and is a

486 proxy of plant and/or soil moisture (Seto *et al.*, 2002). In TCA, the brightness, greenness,  
487 wetness bands are directly associated with physical scene attributes and therefore easily  
488 interpreted (Figure 5). TCA analyses to detect delta morphological change is seldom carried out  
489 alone and is used as a data reduction technique prior to the data being analyzed by another  
490 technique(s). Examples of the usage of TCA is given in section 4.3.

491



492 **Figure 5: A typical representation of earth features between correlations of the three transformed**  
493 **bands.**

### 494 3.1.8 Artificial Neural Networks (ANN)

495 Artificial Neural Networks (ANN), a form of Artificial Intelligence (AI), can be used to semi-  
496 automate image classification, and has become a common alternative to conventional band  
497 statistical approaches. The development of ANNs was inspired from human brain recognition  
498 and brain learning mechanisms (Berberoglu *et al.*, 2000). Neural networks consist of input and  
499 output layers, as well as (in most cases) a hidden layer consisting of units that transform the input  
500 into something that the output layer can use (Foody *et al.*, 1995). They are excellent tools for  
501 finding patterns which are far too complex or numerous for a human programmer to extract and  
502 train the machine to recognize (Samarasinghe, 2016).

503 The backpropagation algorithm (Paola and Schowengerdt, 1995) is the most common method of  
504 training multi-layer networks to date (Samarasinghe, 2016), with an emphasis on its application  
505 to pattern recognition in multispectral imagery. It allows networks to adjust their hidden layers of  
506 neurons in situations where the outcome does not match what the user is hoping for  
507 (Samarasinghe, 2016), similar to a network designed to recognize muddy shores, and  
508 misidentifies them as turbid waters.

509 As delta evolution is a very intricate non-linear process influenced by many factors such as the  
510 coming water and sediment discharges and coastal dynamics, neural networks possess great  
511 robustness over traditional classifiers as neural networks are also inherently nonparametric  
512 nature. The strengths of a neural network lie in arbitrary decision boundary capabilities (the  
513 ability to partition the data set into separate classes effectively), easy adaptation to different types  
514 of data and input structures, possibility of fuzzy output values (probability of a pixel belonging to  
515 a certain information class type) that can enhance classification accuracies (classification  
516 accuracies of fuzzy outputs are discussed in the Fuzzy logic section), and good generalization for  
517 use with multiple images. Land/water rasters created using neural networks are later used with  
518 GIS methods to extract deltaic shorelines. The disadvantages of the method are inconsistent  
519 results due to random initial weights, the requirement of obscure initialization values (e.g.,  
520 learning rate and hidden layer size: the “black box,” phenomenon in which the user feeds in data  
521 and receives answers, and no access to the exact decision making process), slow training time of  
522 the network, and heavy computational demand to train the network for large datasets (Xie *et al.*  
523 2008). For a detailed analysis of advantages and disadvantages of neural networks for remote  
524 sensing applications, the readers are referred to Jarvis and Stuart (1996) and Mas and Flores  
525 (2008). We can conclude from the literature that although the neural network method has several

526 unique capabilities, it will become a useful tool in remote sensing only if it is made faster, more  
527 predictable, and easier to implement.

### 528 3.1.9 *Decision Trees and Random Forest Classifiers*

529 A Decision Tree is a tree-structure like flowchart (Friedl and Brodley, 1997; Figure 6). There are  
530 many different types of decision tree algorithms, e.g. Classification and Regression Tree  
531 Algorithm (CART; Denison *et al.*, 1998), C4.5 (Mazid *et al.*, 2010).

532 Decision Trees are easy to interpret, their internal workings are capable of being observed,  
533 making it possible to reproduce work, while making no statistical assumptions regarding the  
534 distribution of data (Hass and Bun, 2014). They are also computationally efficient (Friedl and  
535 Brodley, 1997), and perform well on large multispectral datasets (Zhang *et al.*, 2017).

536 One of the major problems with using decision trees is overfitting, especially when a tree is  
537 particularly deep (Friedl and Brodley, 1997; Pal and Mather, 2003). Over-fitting occurs when the  
538 tree is designed so as to perfectly fit all samples in the training data set, resulting in branches  
539 with strict rules of sparse data. This affects the accuracy when predicting samples that are not  
540 part of the training set (i.e. yields highly accurate output for the training data but low accuracy  
541 for test data).

542 Random Forest (RF) classifiers mitigate this problem well. First proposed by Breiman (2001), a  
543 RF is simply a collection of decision trees whose results are aggregated into one final result.  
544 Their ability to limit over-fitting without substantially increasing error due to bias makes them a  
545 powerful model. In a random forest, the number of trees in the forest ( $n$  estimators), and the  
546 maximum number of features to be used in each tree can be specified. However, one cannot  
547 control the randomness over which feature is part of which tree in the forest, and there is no

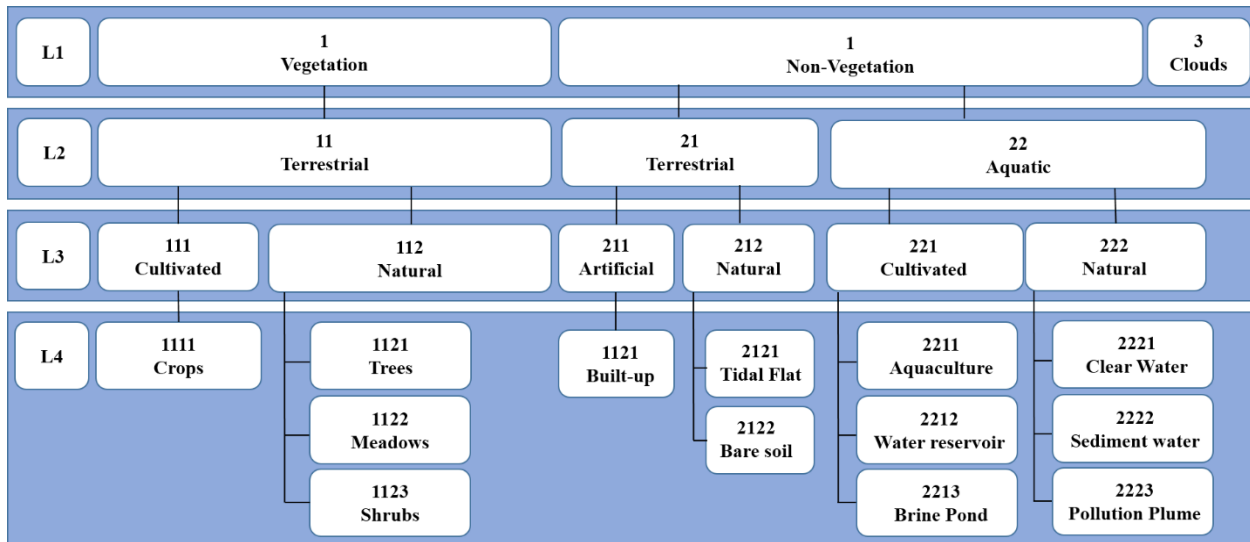
548 control on which data point is part of which tree. Accuracy keeps increasing as the number of  
549 trees is increased but becomes constant at a certain point.

550 RFs can handle both high dimensional data and use a large number of trees where the key issue  
551 is correlation reduction between the random classification variables (ability to handle thousands  
552 of input variables without variable deletion) and they can be run efficiently on large databases.  
553 The RF algorithm can also detect outliers, which can be very useful when some of the cases may  
554 be mislabeled.

555 Random forests have been extensively applied to deltaic image classification and has resulted in  
556 improved classification accuracy compared to traditional methods, such as maximum likelihood  
557 (ML) and artificial neural network (ANN) methods (Adam *et al.*, 2012; Akar and Güngör, 2015).  
558 RFs outperform single decision tree algorithms (Gislason *et al.*, 2006; Khatami *et al.*, 2016).

559 With this combination of efficiency and accuracy, along with very useful analytical tools, the RF  
560 classifier is considered very desirable for multisource classification of remote sensing and  
561 geographic data. That said, RFs are not immune to caveats; they can be time-consuming, difficult  
562 to construct and require greater computational resources in comparison to decision trees. In  
563 addition, since RFs deal with a number of decision trees, and the randomness of features within  
564 decision trees is uncontrollable, there is no way for the user to have a qualitative understanding  
565 of the behavior of the dataset to have an educated guess of the outputs, and therefore, has to take  
566 the output decision of the algorithm at face value.





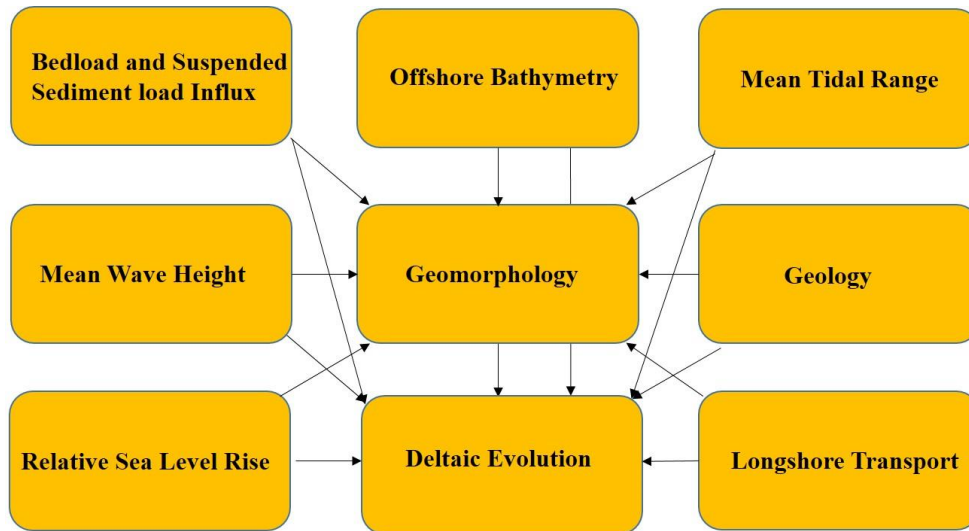
567

568 **Figure 6: A decision tree to characterize different coastal features and isolate the shoreline**

569 *3.1.10 Bayesian Networks*

570 Bayesian networks (BNs), also known as belief networks (or Bayes nets for short), are directed  
 571 acyclic graphs (DAGs) belonging to the family of graphical models (Jensen, 1996). These  
 572 graphical structures include nodes representing the various quantities, variables, or parameters  
 573 that serve as input information, and edges between the nodes (the arrows connecting the nodes)  
 574 representing probabilistic dependencies among the corresponding random variables. A node that  
 575 is not connected shows a variable that is independent by other variables represented by nodes in  
 576 the graph. In comparison to others, this is a relatively new method in deltaic-feature  
 577 identification using remotely sensed imagery. Remotely sensed imagery can be used as input  
 578 information (in contrast to the conventional field collected/modeled databases), and the  
 579 conditional dependencies in the graph are often estimated by using known statistical and  
 580 computational methods. The structure of a DAG in relation to evolution of a delta shoreline is  
 581 illustrated in Figure 7.

582  
583  
584  
585  
586  
587



588 **Figure 7: Bayesian Network to detect deltaic evolution. Black arrows indicate causal relationships**  
589 **linking the forcing factors and the response variable (deltaic evolution)**

590 In Figure 7, the nodes represent random variables and are drawn as boxes labeled by the variable  
591 names. The edges represent direct dependence among the variables and are drawn by arrows  
592 between nodes. In particular, an edge from node “Mean Tidal Range” to node “[Deltaic]  
593 Geomorphology” represents a statistical dependence between the corresponding variables. Thus,  
594 the arrow indicates that a value given to variable “Geomorphology” depends on the value of  
595 variable “Mean Tidal Range”. Given the conditional dependencies, BNs can be effectively used  
596 to represent knowledge about an uncertain domain (e.g. “Deltaic evolution”) and algorithms can  
597 be created that allow for learning and inference through the use of a Bayesian network.

598 Often ANNs are compared to BNs due to their similarities in using directed graphs methods and  
599 are both used as classifier algorithms in problem solving. However, unlike ANNs the BN  
600 structure itself provides valuable information about conditional dependence between the  
601 variables. It is a visual representation of graph that is vertices and edges have meaning in  
602 comparison the ANNs where the network structure does not offer direct interpretations between

603 nodes and can be difficult to interpret. Not many studies are found in literature which use BNs  
604 exclusively for deltaic feature detection (Table 2), primarily due to the large amount of  
605 supplementary data needed to setup such networks.

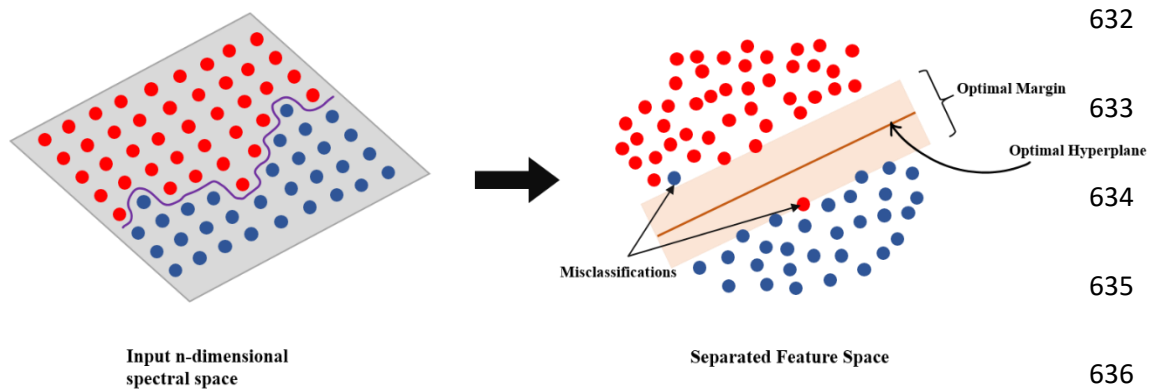
### 606 *3.1.11 Support Vector Machines*

607 A Support Vector Machine (SVM) is a machine-learning technique that is useful for  
608 multispectral and hyperspectral remotely-sensed classifications in which spectral separability  
609 between coastal land and water is difficult to ascertain due to lack of clear zonation between  
610 vegetation species, and mixed pixel effects. SVM differs from traditional classification  
611 approaches by identifying the boundary between classes in n-dimensional spectral-space rather  
612 than assigning points to a class based on mean values of class clusters (Heumann, 2011).

613 SVM creates a hyperplane through n-dimensional spectral-space that separates classes based on a  
614 user defined kernel function and parameters that are optimized using machine-learning (Figure  
615 8). In other words, given labeled training data, the algorithm outputs an optimal hyperplane  
616 which categorizes new feature classes (Figure 8). In two-dimensional space this hyperplane is a  
617 line dividing a plane in two parts where each class lays either side of the hyperplane. By  
618 identifying the hyperplane that separates two classes rather than using the distance between class  
619 spectral means, SVM can produce a more accurate classification.

620 Several studies have demonstrated the great potential of SVM. Pal and Mather (2005) found that  
621 SVM outperforms maximum likelihood and artificial neural network using Landsat TM and is  
622 well suited for small training sets and high-dimensional data. Foody and Mathur (2006) found  
623 SVM outperforms discriminate analysis and decision-tree algorithms for airborne sensor data. Li  
624 *et al.* (2010) applied SVM to an Object-based Image Analysis (OBIA) with better results than

625 standard fuzzy logic classification. Elhag *et al.* (2013) used Landsat TM and ETM+ imagery to  
 626 map landcover in the Nile River Delta using SVM and Supervised classification approaches and  
 627 showed that SVM showed higher classification accuracies. Thanh Noi and Kappas (2018)  
 628 concluded that the SVM classifier on average outperformed the Random forest and kNN (K-  
 629 nearest neighbor (unsupervised)) classifiers. Given the success in the literature (see examples in  
 630 Table 2), we can conclude that SVM as the best individual classification technique for  
 631 morphology change detection amongst pixel-based classification techniques.



637 **Figure 8: An Illustration of the SVM concept**

638 *3.1.12 Object-based Image Analysis (OBIA)*

639 Traditional pixel-based image classification assigns a land cover class per pixel. All pixels are  
 640 the same size, same shape and do not have any implicit connectivity with of their neighboring  
 641 cells. OBIA, on the other hand, segments an image by grouping small pixels together into vector  
 642 objects. The OBIA is a two-step process: segmentation and classification. Segmentation breaks  
 643 up the image into objects representing land-based features. These segmented objects become the  
 644 unit of analysis, from which spectral statistics, such as spectral band means and standard  
 645 deviation, or spatial information, such as image texture, can be used in the second process; image  
 646 classification. In image classification, according to the spectral, temporal and spatial response of

647 land cover types in the objects, the corresponding bands and band combinations are selected, and  
648 their sensitivity is trained.

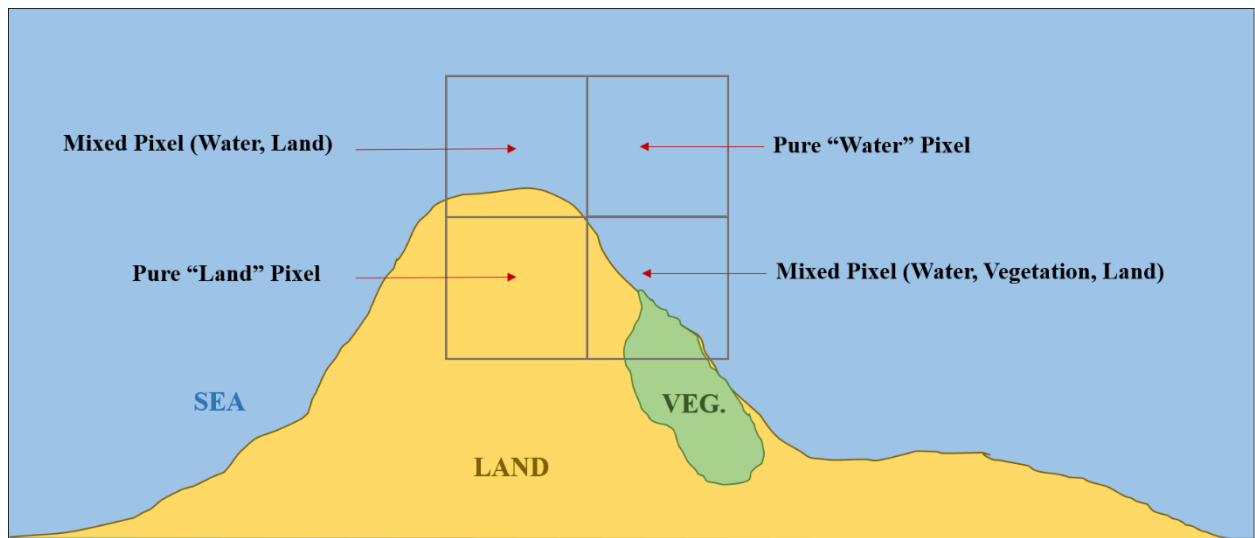
649 Object Based Image Analysis is conceptually simple and generic across sensors (Blaschke,  
650 2010). The key benefits of OBIA relative to pixel-based methods include: (1) the possibility to  
651 incorporate user-defined scale, shape, and compactness parameters useful for creating objects  
652 with heterogeneous pixels (in the process of creating objects, scale determines the occurrence or  
653 absence of an object class, and the size of an object affects a classification result), in addition to  
654 spectral values of the input image layers (Blaschke, 2010); (2) smoothing some of the local  
655 variation within objects, which may reduce the salt-and-pepper noise and enhance classification  
656 accuracy (Kamal and Phinn, 2011; Kim *et al.*, 2011); and (3) accounting for the landscape  
657 hierarchy of patch, cover type and ecosystem structure by working with multiple object layers  
658 nested within each other at different spatial scales (Krause *et al.*, 2004). The approximation of  
659 ground entities and patches by image objects makes them more ecologically relevant and  
660 potentially more resilient to minor geospatial positioning and image registration error than pixel  
661 units (Yoshino *et al.*, 2014).

662 Drawbacks include spectral similarity of diverse classes due to homogenizing effects of moisture  
663 or dead vegetation signals, and dilution of fine morphological features which may reduce  
664 classification accuracy and the effectiveness of class discrimination (Kamal and Phinn, 2011;  
665 Yoshino *et al.*, 2014).

666 **3.1 (B) Sub-pixel-based methods**

667 Most classification approaches, as discussed above, are based on per-pixel information, in which  
668 each pixel is classified into one category and the land-cover classes are mutually exclusive.

669 However, in the highly turbid coastal zone, waters are mixed with various materials including  
670 suspended particles, sediments and phytoplankton, and can often be classified as “land” in many  
671 conventional algorithms. In addition, classification accuracies decrease when there is more than  
672 one land cover type within a given pixel (Figure 9), making it a challenging task to correctly  
673 classify new land growth and shoreline with shoal waters.



674

675 **Figure 9: The case of the ‘mixed pixel’**

676 A relatively young field in image analysis, and one that has gained traction over the past decade  
677 or so, Sub-pixel representations, provide the opportunity to extract information about the fraction  
678 of different classes within a mixed pixel (soft classification). Soft Classification approaches in  
679 general were shown to result in improved cartographic representations of transitional zones and  
680 heterogeneous landscapes (Frohn *et al.*, 2012; Wei *et al.*, 2008; Zhang, 2009). There are three

681 main types of soft classification approaches used in delta morphology studies currently: Fuzzy  
682 Logic, Spectral Mixture Analysis, and Sub-Pixel Analysis.

### 683 *3.1.13 Fuzzy Logic*

684 A fuzzy classification technique is a probability-based classification rather than a hard  
685 classification. It was shown to be an extremely useful classification technique in deltaic regions  
686 where the identification of the shoreline is challenging due to the shallowness and turbidity of  
687 water, vegetative gradients, and dynamically changing waterline (Zhu, 2001). A fuzzy  
688 classification allows a pixel to have multiple and partial class memberships to accommodate the  
689 effects of mixed pixels. The conventional output of a fuzzy classification is a set of fraction  
690 images which indicate the relative coverage of the classes in the area represented by the pixel. If  
691 these predicted class covers could be located geographically within the area represented by the  
692 pixel, it would allow the boundary between classes to be plotted at a subpixel scale.

693 Fuzzy classification has advantages over conventional methods and improves drastically on the  
694 classification accuracies by fuzzy partitioning as the spectral space and retaining information  
695 otherwise would have been lost due to conventional partitioning and classifier training.

696 Ghanavati *et al.* (2008) showed a better performance of fuzzy classification over maximum  
697 likelihood classification and also showed better discrimination of mixed and unmixed land  
698 use/land cover categories. It is also more feasible in integrating remotely sensed data and  
699 ancillary data (Zhang & Foody, 1998; Sha *et al.*, 2008) such as digital elevation models, channel  
700 networks and climate data (Lu and Weng, 2007). However, fuzzy classifications can be very  
701 slow with long run-times during feature classifications when higher accuracies are sought after.  
702 This is because additional fuzzy rules have to be incorporated into the system, and algorithms

703 need to be tweaked (since they do not use training data) to solve for complex deltaic  
704 environments.

#### 705 *3.1.14 Spectral Mixture Analysis*

706 Spectral mixture analysis (SMA) enables the extraction of information about the surface  
707 materials present in a pixel. This is done by calculating the least-squares best fit for each pixel  
708 along mixing lines bounded by spectra of end-members and in this way accounts for each pixel's  
709 variation in the mixture composition (Ozesmi and Bauer, 2002). An end-member ideally  
710 represents a pure component of the mixtures present in the pixels.

711 The output of SMA is typically presented in the form of fraction images, with one image for each  
712 end-member spectrum, representing the area proportions of the end-members within the pixel.

713 End-member selection is one of the most important aspects in SMA, and much previous research  
714 has explored selection/identification approaches (Mustard and Sunshine, 1999; Theseira *et al.*,  
715 2003; Small, 2004).

716 Previous research has demonstrated that SMA is helpful for improving classification accuracy  
717 (Shimabukuro *et al.*, 1998; Lu *et al.*, 2003) and is especially important for improving area  
718 estimation of land-cover classes based on coarse spatial resolution data. Albeit its increased  
719 accuracy over other methods, SMA suffers from two major caveats of 1) not having potential  
720 end-members occurring in patches larger than the image resolution; there could exist earth  
721 features in smaller patches smaller than pixel dimensions. This makes the identification of an  
722 end-member for classification impossible and consequently be classified erroneously. 2) end-  
723 members not being truly constant within an image; there always exist a range of reflectance  
724 values for a particular end-member class that could result in overlap between different end-



725 member classes. This could create a mismatch between the defined end-member and ground  
726 truth and yield misclassification results.

### 727 *3.1.15 Sub-Pixel Analysis*

728 Sub-pixel processing is defined as the search for specific materials of interest from within a  
729 pixel's mixed multispectral image digital number spectrum. This method has advantages over  
730 SMA and fuzzy classifications, because the overall composition of each pixel is not limited to a  
731 combination of already defined image classes (end-members). The steps in sub-pixel processing  
732 include signature derivation for a material of interest and classification of each pixel identifying  
733 the fraction of material of interest present. Therefore, for each material a separate classification  
734 must be done. The fraction image pixel values vary from 0.0 to 1.0 (Ozesmi and Bauer, 2002).  
735 This specific technique of sub-pixel analysis in deltaic environments was the least used  
736 technique in the reviewed literature.

### 737 *3.1.16 General Concerns about Techniques used in Two-Step Change Detection*

738 The 15 techniques used in Two-Step Change Detection for delta morphology analysis described  
739 above, although commonly used, share some inherent limitations. One limitation is that since  
740 separate classifications are carried out on two different satellite images before detecting the  
741 deltaic change, the accuracy of the change map typically will be at best the multiplication of the  
742 accuracies of each individual classification for each date (Serra *et al.*, 2003). This is a concerning  
743 problem as this error can be significant at times, especially when multiple time steps are  
744 compared. Also, when the analyses include utilization of imagery from longer archives (i.e. use  
745 of different Satellites even in the same constellation; e.g. Landsat MSS, TM etc.), it is inevitable  
746 that different data extraction and classification algorithms needed to be used to infer deltaic

747 features (due to the variability of spectral resolution of bands). This process, in addition to the  
748 caveat mentioned above, carries the distinct disadvantage of having uncertainties occurring due  
749 to differing classification/extraction algorithms. Thus, the two-step detection will incur an  
750 additional step of quantifying of uncertainties.

751 Furthermore, Two-Step Change Detection, since it requires the production of at least two  
752 different maps, can be operationally complex and computationally intensive (especially on high  
753 resolution multispectral imagery covering large areas). Therefore, the use of said methods to  
754 produce time series of change-maps can be difficult and expensive. Multi-temporal image  
755 comparison techniques/One-step change detection techniques (discussed below) were, in part,  
756 developed to alleviate these limitations.

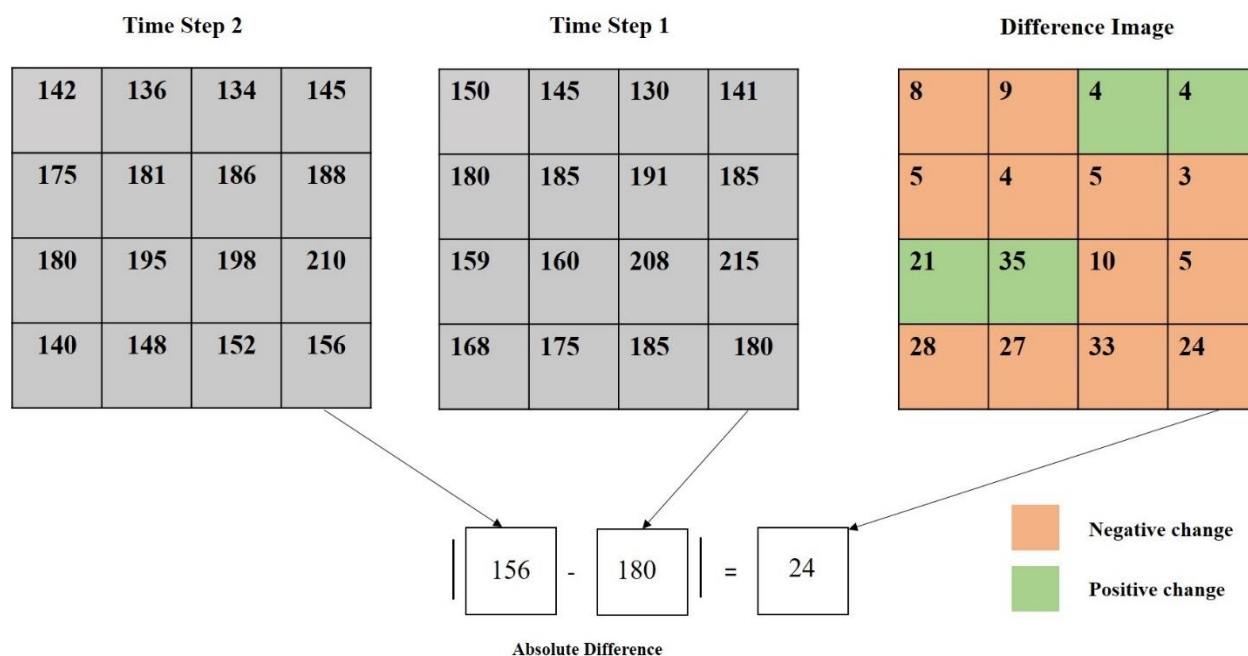
## 757 **3.2 Classification Techniques used in One-Step Change Detection**

### 758 *3.2.1 Image Differencing/Layer Arithmetic*

759 In this technique, spatially registered images from different times are subtracted, pixel by pixel,  
760 to produce a layer which represents the change between the two. This procedure yields a  
761 difference distribution for each band (i.e. a histogram). In such a distribution, pixels of small  
762 radiance change are distributed around the mean, while pixels of large radiance change are  
763 distributed in the tails of the distribution (Mas, 1999). A critical element of the image  
764 differencing method is deciding where to place the threshold boundaries between change and no-  
765 change pixels displayed in this distribution.

766 Although Image Differencing is a widely used technique for change detection and has been used  
767 in river deltas of different geographical environments (Table 2), interpreting the difference image  
768 can be difficult because different input values can have similar output results after subtraction

769 (e.g. input pixel values of 190 and 150 can have the same result of 40, as inputs of 100 and 60,  
 770 after subtraction), and also since the original pixel value information is not retained for further  
 771 investigations (Cohen *et al.*, 1998). The mathematics of typical image differencing is shown in  
 772 Figure 10 below.



773 **Figure 10: Image differencing workflow between typical rasters. The values are arbitrary values**  
 774 **used for illustration purposes.**

### 775 3.2.2 Change Vector Analysis

776 Change Vector Analysis (CVA) is an enhanced version of band differencing. It detects changes  
 777 above a selected threshold value to generate a binary image of change and no-change pixels  
 778 (Singh and Talwar, 2013). A change vector can be described as an angle (vector direction) and a  
 779 magnitude of change between two different time instances from multi-spectral satellite data  
 780 (Civco *et al.*, 2002). A decision on change is made based on whether the change magnitude  
 781 exceeds a specific threshold. Once a pixel is identified as changed, the direction can be examined  
 782 further to determine the type of change. The type of change is often identified using the angle of

783 the vector in two spectral dimensions (Chen *et al.*, 2003). Although initially developed for only  
784 two spectral bands, modifications to CVA enable its use to any number of spectral bands  
785 (Bayarjargal *et al.*, 2006).

786 In addition to providing the direction of change, which is unparalleled to other techniques  
787 discussed, CVA also has the capability of avoiding cumulative error in image classification of an  
788 individual date and processing any number of spectral bands simultaneously to retrieve  
789 maximum “from-to” type information. However, like other radiometric change approaches, CVA  
790 also has several drawbacks that limit its use. These include a strict requirement for reliable image  
791 radiometry. CVA is based on pixel-wise radiometric comparison and so the accuracy of image  
792 radiometric correction (for alleviating the impacts caused by disturbing factors such as different  
793 atmospheric conditions, solar angle, soil moisture and vegetation phenology, etc.) is more critical  
794 for CVA than for spectral classification approaches. Another drawback is a lack of automatic or  
795 semiautomatic methods to effectively determine the threshold of change magnitude between  
796 change and no-change pixels (Chen *et al.*, 2003).

### 797 **3.3 Ensemble Classifications**

798 Different image classification methods, such as parametric classifiers (e.g. maximum likelihood)  
799 and non-parametric classifiers (e.g. neural networks, decision trees), have their own strengths  
800 and limitations (Tso and Mather, 2001). For example, when sufficient training samples are  
801 available and the features in a dataset are normally distributed (distribution in space; among  
802 pixels), a maximum likelihood classifier (MLC) may yield an accurate classification result. In  
803 contrast, when image data are anomalously distributed, neural network and decision tree  
804 classifiers may demonstrate a better classification result (Lu *et al.*, 2004).

805 Ensemble (Hybrid) classification methods combine the strengths of multiple classification  
806 approaches. They can be valuable for river delta studies because of how they effectively address  
807 the complex variability in spectral responses of shoreline environments. Ensemble classifications  
808 can be classified into two approaches: 1) classifying a single image of a particular time step and  
809 then comparing it with an image of a different time step (classified using the same techniques or  
810 otherwise), or 2) directly comparing between two timestamps. The direct comparison between  
811 time steps is often expressed as a layer arithmetic operation to identify changed elements  
812 (locating change through e.g. CVA), followed by a supervised or unsupervised direct  
813 classification of the changed features (Lu *et al.*, 2004). Previous research has indicated that the  
814 integration of two or more classifiers provides improved classification accuracy compared to the  
815 use of a single classifier (Warrender and Augusteihn, 1999; Steele, 2000; Huang and Lees, 2004;  
816 Khatami *et al.*, 2016). In an effort to not duplicate studies and maintain the succinctness of the  
817 document, the readership is reverted to sections discussed above (3.1.1 – 3.1.15; 3.2.1 and 3.2.2)  
818 where instances of ensemble classifications can also be found. A note of caution when applying  
819 ensemble classifications is that the uncertainties occurring from different techniques have to be  
820 quantified and factored into accuracy calculations of feature extractions, as they can be  
821 significant depending on the methods used and the number of time steps of satellite imagery  
822 processed.

823 As evident from the discussion in sections 3.1-3.3, sub-pixel-based classifications tend to yield  
824 better results than pixel-based classifications. However, sub-pixel-based methods can be  
825 computationally expensive, and algorithm development can be time consuming. Thus, the choice  
826 of a sub-pixel-based algorithm is a trade-off between how complex the deltaic environment is,  
827 how big the river delta is (i.e. is the value of a pixel significant in comparison to the size of the

828 delta?), and what is the time span of the delta change analysis (are multiple image time steps  
829 involved which could compound uncertainties). In addition, since there is also the problem of  
830 compounding error resulting from classification techniques of different time steps, development  
831 of algorithms to detect sub-pixel heterogeneity can be worthwhile if a one-step change detection  
832 method, even pixel-based (e.g. image differencing. CVA), can achieve comparable results as  
833 sub-pixel algorithms.

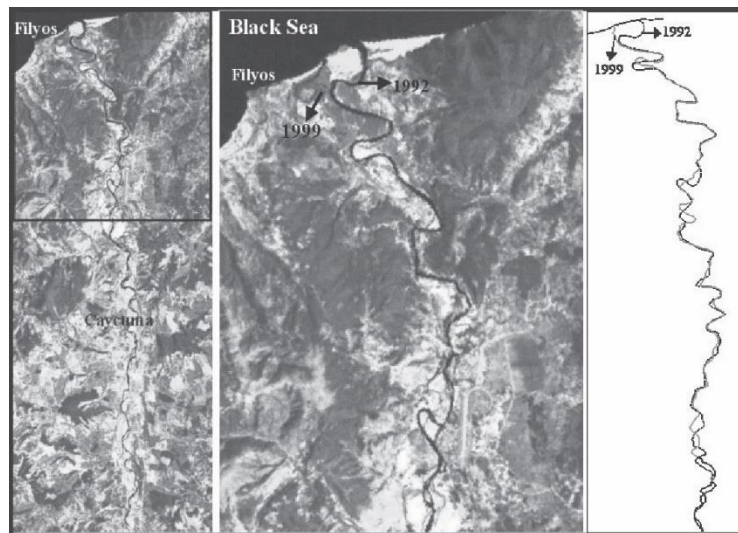
#### 834 **4. Other Delta Morphology Change Indicators**

835 Section 3 of the manuscript focused on one delta morphology change indicator: the shoreline.  
836 The discussion of all other environmental indicators in one section is due to that fact that the  
837 number of studies pertaining to every other environmental indicator was markedly less than  
838 those for deltaic shoreline change studies. We attribute this to two reasons 1) research interest:  
839 more attention is given to how deltaic landmass available for humans evolve over time (governed  
840 by the shoreline), and 2) methodological challenges: difficulty for classification algorithms to  
841 distinguish between spectral characteristics of these specific deltaic features and the surrounding  
842 terrain features. The shoreline, on the other hand, even with its own complexities at the land-sea  
843 margin, is relatively easier to detect, as changes in spectral characteristic between land and sea  
844 are comparatively prominent. Possible pathways to address these less-researched environmental  
845 indicators are discussed as future directions in section 5. The following sub-sections will discuss  
846 studies with regard to other deltaic morphology change indicators. The importance and role of  
847 these indicators in delta morphology change detection is summarized in Table 1.

848 **4.1 Meander Belts**

849 Lateral migration as a response to variations in river flow and sediment discharges is associated  
850 with erosion of the stream bed or channel bank and can cause many geomorphological and river  
851 management problems on a delta (Le *et al.*, 2006). Mathers and Zalasiewicz (1999) used a  
852 combination of filtration and contrast stretching on Landsat TM imagery to map and classify  
853 Meander Belts of the Red River in the Red River Delta in Vietnam. Yang (1996) and Yang *et al.*  
854 (1999) used Manual Digitization and Band Ratioing/Manual digitization on Landsat MSS and  
855 TM imagery to identify channel shifting change (Channel Migrations), channel geometric change  
856 (Channel length and width) and channel pattern change (braiding, straight, slight meandering) of  
857 the Yellow River in the Yellow River Delta. Seker *et al.* (2005) studied meander migrations of  
858 the Filyos River in and upstream of the Filyos delta, Turkey (Figure 11) and Ghanavati *et al.*  
859 (2007) used topographic maps and Landsat TM and ETM+ imagery to detect channel migrations  
860 in the Hendijan River delta, Iran.

861  
862  
863  
864  
865  
866



867 **Figure 11: The meandering of the Filyos River through time observed using satellite imagery.**

868 **Source: Seker *et al.* (2005).**

869 **4.2 Crevasse Splays, Channel Avulsions and Distributary Networks**

870 Syvitski *et al.* (2012) used SRTM (Shuttle Radar Topography Mission) interferometric synthetic  
871 aperture radar (InSAR) data to study zones of nodal avulsions in 33 lowland floodplains  
872 (inclusive of deltas). Li *et al.* (2014) used Landsat MSS and TM imagery, and Li and Bristow  
873 (2015) used QuickBird-2 and WorldView-2 imagery to monitor flood-induced river morphology  
874 changes and to study splay development morphology respectively in the Río Colorado river delta  
875 in Salar de Uyuni, Bolivia (Figure 12). Mathers and Zalasiewicz (1999) used Landsat TM with  
876 the integration of geological data to study tidal creeks, channels, anastomosing rivers in the Red  
877 River Delta, Vietnam. Isikdogan *et al.* (2015) proposed an algorithm to automatically extract the  
878 channel networks from satellite imagery where water and non-water pixels have the greatest  
879 spectral contrast, and in an innovative use of high resolution google earth imagery, Gugliotta *et*  
880 *al.* (2019) obtained channel network widths and sinuosity of five deltas (Fly, Yangtze, GBM,  
881 Irrawaddy, and Mekong).

882

883

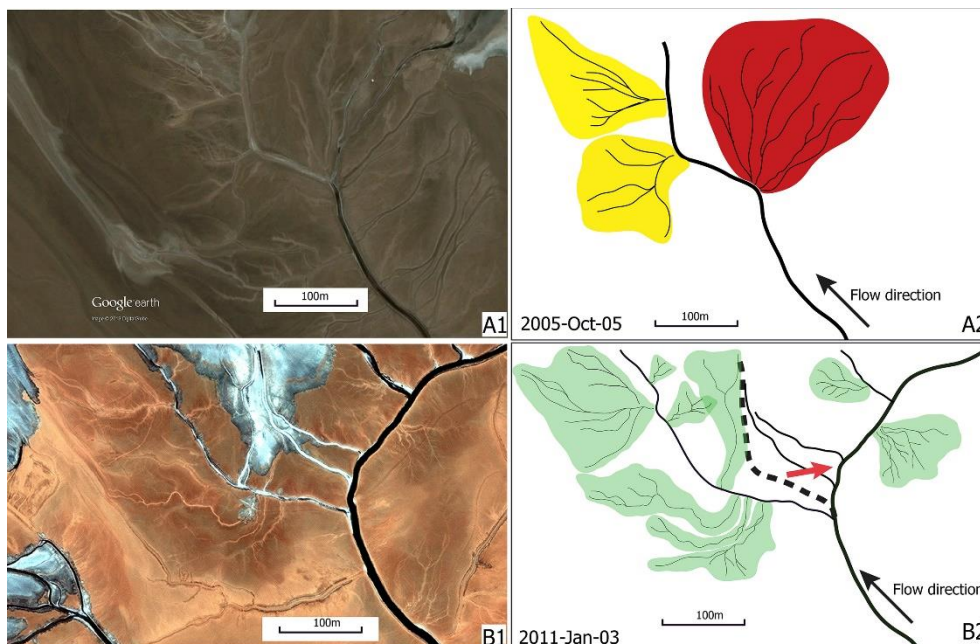
884

885

886

887

888





889 **Figure 12: Crevasse splay-led avulsion in the Salar de Uyuni, Bolivia. A1 and B1: The same region**  
890 **observed from Quickbird (A1) and Worldview-2 (B1) satellites at two different times; A2 and B2:**  
891 **Line drawings, main river channel is demarcated by the thick black line. A2: yellow splays**  
892 **represent Inactive Crevasse Splays; red splay demarcates the site where avulsion occurs. B2: green**  
893 **splays represent new crevasse splays. Dashed line indicates river channel before avulsion. The**  
894 **arrow shows the channel shift after avulsion. Source: Li and Bristow (2015).**

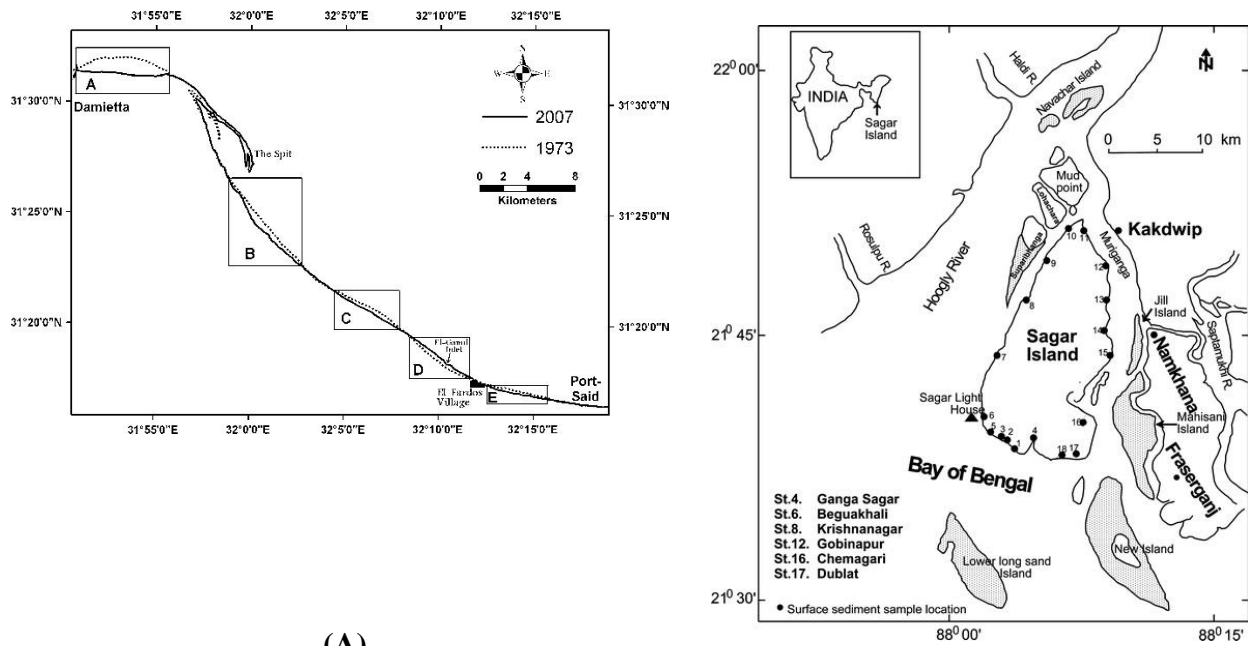
895 Studies of splays, avulsions and channel networks is particularly challenging in coastal deltas  
896 due to low topographic gradients, the presence of features such as sediment plumes, and the wide  
897 range of scales over which channel features are present. Channel networks identified in most of  
898 the studies were as good as the moderate resolution of the satellite imagery used. In addition,  
899 robust channel extraction methods would ease monitoring coastal areas and analyzing deltaic  
900 response to anthropogenic and natural forcing over large spatial areas and long temporal  
901 intervals. The role of higher resolution satellite imagery in better identifying these deltaic  
902 features and the need for more robust deltaic feature extraction methods based on these better  
903 platforms is discussed in section 7.

#### 904 **4.3 Barrier Islands, Beach Spits, and Mouth Bars**

905 Frihy *et al.* (1998) used Landsat satellite data to assess the evolution of the coastal spit and  
906 changes in the lagoon margin and contiguous barrier islands in the Damietta Promontary of the  
907 Nile River Delta. Nandi *et al.* (2016) used Tasseled Cap Transformation on Landsat MSS, TM,  
908 ETM+ while Gopinath and Seralathan (2005) used image differencing on satellite data of the  
909 Indian Remote Sensing Satellite-IC to monitor changes of Sagar Island, the largest mouth bar of  
910 the Ganga-Brahmaputra-Meghna (GBM) delta. Demers *et al.* (2015) used RADARSAT-2 C-  
911 band and optical satellite data to map the shoreline of islands of the outer Mackenzie Delta using

912 Object Based Image Analysis. A common problematic are highlighted in these studies was  
 913 detecting these morphological features using medium to coarse resolution imagery. Better pixel  
 914 resolutions in comparison to the scale of deltaic features (Figure 13) were shown to be an area of  
 915 improvement for better feature detection. In addition, the detections were heavily impaired by  
 916 the sediment plume in the delta nearshore environment. The necessity of data mining and sub-  
 917 pixel analyses was apparent. We discuss these shortcomings and possible pathways forward in  
 918 detail in section 7; Future Directions.

919



920

921

922

923

924 **Figure 13: (A) The shoreline position change through time (1973 and 2007) between Damietta and**  
 925 **Port-Said of the Nile River Delta. A prominent beach spit is visible between locations A and B.**  
 926 **Source: El-Asmar and Hereher (2011). (B) Location of The Sagar Island, the largest barrier Island**  
 927 **in the Ganges-Brahmaputra-Meghna Delta. Ground control points were collected at each sampling**  
 928 **station to calibrate satellite data. Source: Gopinath and Seralathan (2005).**

## 929 5. Synthesis and Applications

### 930 5.1 Machine Learning

931 One of the major insights stemming from this literature review is that sub-pixel-based methods  
932 tend to yield the highest accuracies among all the discussed methods in morphology change  
933 detection, while machine learning (ML) techniques perform relatively better (contingent upon  
934 good training data, and knowledge and skill of the algorithm developer) than conventional pixel-  
935 based techniques (band ratioing, density slicing). The former is a straightforward conclusion  
936 given that sub-pixel-based methods inspect details within the constraints of a pixel to elucidate  
937 information about the land surface which is otherwise impossible through pixel-based methods;  
938 higher level of inspection within a pixel will yield greater amounts of detail.

939 Perhaps more interesting is the insight that ML techniques (e.g. ANNs, Bayesian networks etc.)  
940 perform better than conventional methods, given that they both work at a pixel-level. It is also  
941 found that using a combination of ML techniques with others (another ML technique or other  
942 conventional ones) was shown to yield very high accuracy and utility in morphological feature  
943 classification. Thus, it is worthwhile examining why ML techniques perform well in deltaic  
944 environments, so we could better understand and harness their strengths to developing data  
945 mining algorithms in under-studied deltaic regions of the world, and even solve image  
946 classification issues in other sub-disciplines of satellite remote sensing.

947 The reasons for the success of ML techniques in case studies in the studied literature lie in the  
948 complexity of the deltaic system itself. One of the fundamental characteristics of a complex  
949 system is that classification results are non-linear stemming from the heterogeneity in the system  
950 (a spectral reflectance of  $x$  denoting water at one location, might be a mixture of mud, water and

951 vegetation debris, at another). A conventional algorithm is designed to classify the system using  
952 a simple succession of steps subject to simple conditions. ML algorithms, on the other hand,  
953 have the ability to identify complex relationships through the testing of a very large number of  
954 possibilities. Typically, the algorithm runs multiple experiments of classification on the primary  
955 image data before arriving at a final decision output. The outcome of the second experiment will  
956 not be the same as the first, and the final result is thus an ensemble of the two. ML algorithms  
957 work on the principle that it generally approximates the truth instead of aiming to find it exactly,  
958 in comparison to conventional methods, which in a complex domain such as a delta, can lead to  
959 lowered accuracies due to misclassification. The approximation of the truth of ML techniques,  
960 thus, also provide a measure of uncertainty, and can act as platforms for other types of research  
961 to build up on, which can later-on be incorporated into the decision-making process. Secondly, in  
962 a ML algorithm, many other factors related to morphology change are considered before  
963 assigning a label to a particular image pixel (e.g. see Figure 7 of how a Bayesian network solves  
964 for a deltaic evolution). This provides ancillary data (remotely sensed or not) of the deltaic  
965 environment, which improves the classification accuracy of the algorithm.

966 We understand that not every researcher engaged in remote sensing possesses the skills of  
967 developing complex ML algorithms. Therefore, we would also like to make a point that although  
968 ML algorithms are favorable, a combination of conventional methods in an ensemble could also  
969 lead to good classification accuracies.

970 What type of algorithm should one use for delta morphology detection? Is it worth the effort of  
971 going the entire distance of developing highly accurate, complex ML algorithms when,  
972 comparable results can be achieved through already existing conventional remote sensing  
973 techniques? The answer to these questions, in our opinion, depends on several factors. The most  
974 important is the study domain of interest. For example, the Damietta and Rosetta Promontaries of  
975 the Nile River Delta, Egypt (which are made of the Damietta and Rosetta branches of the Nile  
976 River, respectively) are cusped shaped, with straight forward land-sea margins (Figure 14a).  
977 Due to the clear difference in spectral signatures the deltaic land can be clearly distinguishable  
978 from the ocean. On the contrary, the Ganges-Brahmaputra-Meghna (GBM) delta in  
979 India/Bangladesh has intricate coastal features on the land-sea margin (Figure 14b). The  
980 extensive anastomosis of channels, huge volume of sediment output, complex vegetation  
981 gradient, presence of barrier islands, mouth bars and lagoons at the land-sea interface  
982 complicates the detection of morphological features.



983 **Figure 14: The comparisons of shorelines between the (a) Damietta Promontary of the Nile River**  
984 **Delta and the (b) Ganges-Brahmaputra-Meghna Delta**

985 Therefore, it would be prudent to use a combination of conventional techniques to monitor the  
986 Nile, in order to utilize available resources (time, user-skills) effectively rather than going the  
987 extra step of deep algorithm development, which might be very well the case for the GBM delta.  
988 It is therefore of utmost importance to have an understanding of the complexity of the study  
989 domains prior to the development of research methodology. It is also important to be informed  
990 how of data-intensive and computationally costly these algorithms are. For example, a Bayesian  
991 network might be significantly better than a simple band ratio, but is it worth the trade-off of  
992 time that one would invest to develop the algorithm and the amount of ancillary data (which  
993 might need to be purchased and pre-conditioned) that is required to arrive at a relatively  
994 uncomplicated feature extraction?

## 995 **5.2 Radar Imagery**

996 Literature about the use of Radar imagery for deltaic morphological feature detection was  
997 minimal compared to optical platforms. This is likely due to a combination of factors. The first is  
998 the premium access that was needed for almost all radar archives until very recently. Research  
999 proposals on intended projects had to be submitted to data providing agencies, and on most  
1000 occasions, imagery had to be purchased. Secondly, unlike the lengthy activation periods of  
1001 optical platforms (e.g. Landsat, since 1972) the discontinuation of radar platforms within a short  
1002 period of time has led to short archival length of radar imagery which consequently resulted in  
1003 difficulty in monitoring deltaic changes over time. Thirdly, skilled photogrammetric operators  
1004 are needed to process and analyze radar imagery, and these skills are not ubiquitous. Fourthly,  
1005 and most importantly is the utility in distinguishing on-land deltaic features such as crevasse  
1006 splays and avulsions, especially in complex deltaic regions. Although radar imagery is well  
1007 utilized in shoreline delineation (see examples in Table 2), there is no conclusive evidence that

1008 suggests that Radar imagery performs well in comparison to optical imagery in recognizing on-  
1009 land deltaic features. Thus, given the choice between optical and radar platforms, the rational  
1010 selection seemed to be optical imagery over the years in most cases. However, with open  
1011 accessibility policies to radar archives through the Copernicus Program of the European Union,  
1012 Alaska Satellite Facility and the Japan Aerospace Exploration Agency (JAXA), and training  
1013 programs/Webinars offered by NASA, European Space Agency and other private institutions,  
1014 opportunities in relation to feature detection are expected to open into the future.

## 1015 **6. Intercomparison of Delta Morphology Feature Extraction Techniques**

1016 One of the more important insights that we draw from the summation of studies is that the  
1017 review of literature revealed no clear clustering of a particular set of technique(s) that could be  
1018 used for feature extraction for a particular type of delta (e.g. river-dominated vs. tide-dominated).  
1019 One or two given techniques which were used to extract a particular morphological feature (e.g.  
1020 shoreline) of a particular type of delta (e.g. river-dominated delta) was not necessarily ideal for a  
1021 river dominated delta elsewhere on the earth. This is understandable as deltaic morphology  
1022 dynamics are driven by many other location/climate related factors (e.g. inherent variability in  
1023 rainfall, soil minerals, growing cycle phases of vegetation) that make the identification of  
1024 morphological features even using the same technique complex. We noted that there were not  
1025 enough comparison studies which 1) compared multiple techniques at a given case study, nor 2)  
1026 comparisons of even one or two techniques across multiple case studies in different geographical  
1027 regions of the world. The notion of which technique(s) would be the most appropriate for a given  
1028 deltaic region would be immensely important for potential future research as these could be used  
1029 to infer on how to fine tune algorithms to compensate for environmental noise, and subsequently

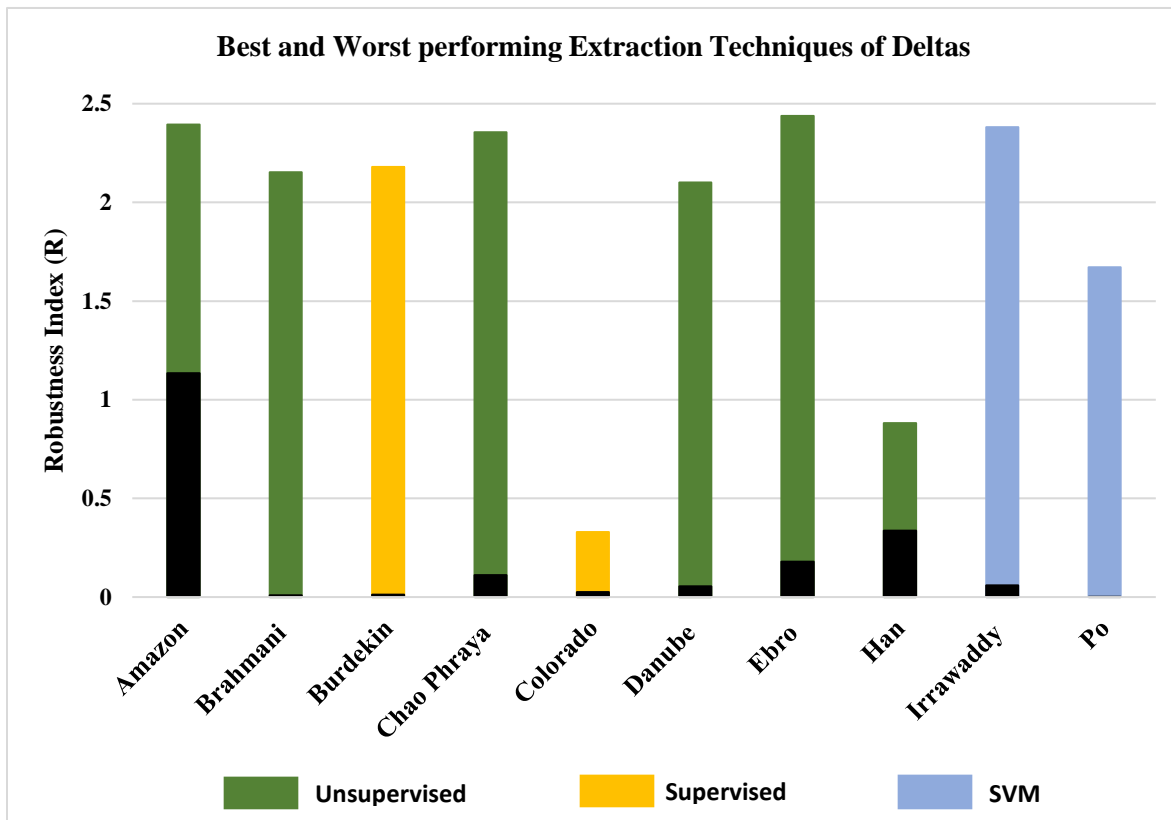
1030 accurately detect deltaic landmass evolution over time. This will help us infer why particular  
1031 techniques underperform in differentiating earth features in different geographic regions of the  
1032 world, enabling deeper investigation into some of the inherent problems of particular techniques  
1033 and provide a platform for their improvement. In addressing this niche, we evaluated 7  
1034 techniques on 10 different river deltas (Amazon, Chao Phraya, Burdekin, Brahmani, Po, Danube,  
1035 Ebro, Han, Irrawaddy, Colorado) globally, belonging to different river delta types (i.e. river-  
1036 dominated, tide-dominated, wave-dominated) and representing the different Köppen climate  
1037 classes.

1038 Five conventional and two ML methods were compared. The conventional methods are: 1)  
1039 Modified Normalized Difference Water Index (MNDWI), 2) Normalized Difference Water  
1040 Index (NDWI), 3) PCA analysis, 4) Unsupervised Classification, and 5) Supervised  
1041 Classification)]. The ML techniques used are: 6) Random Forest Classifier, and 7) Support  
1042 Vector Machine)]. These seven techniques were selected as they were the most used as per our  
1043 review. All were compared against hand-digitized vectors (used as a reference baseline) of  
1044 Landsat-OLI 2018 imagery for the 10 case study deltas (the number of case studies were  
1045 constrained by the availability of sufficient training data for ML techniques). The accuracy of  
1046 different indicators of morphology (shoreline, beach spits, mouth bars etc.) were evaluated  
1047 against the hand-digitizations based on two parameters: a) the continuity of the technique-  
1048 derived vector to the reference baseline, and b) Proximity of technique-derived vector to the  
1049 reference baseline. A new robustness index ( $R$ ) was developed which joins both metrics:

1050 
$$R = \frac{L_E * 100 / L_R}{D_{EA}} \quad (1)$$

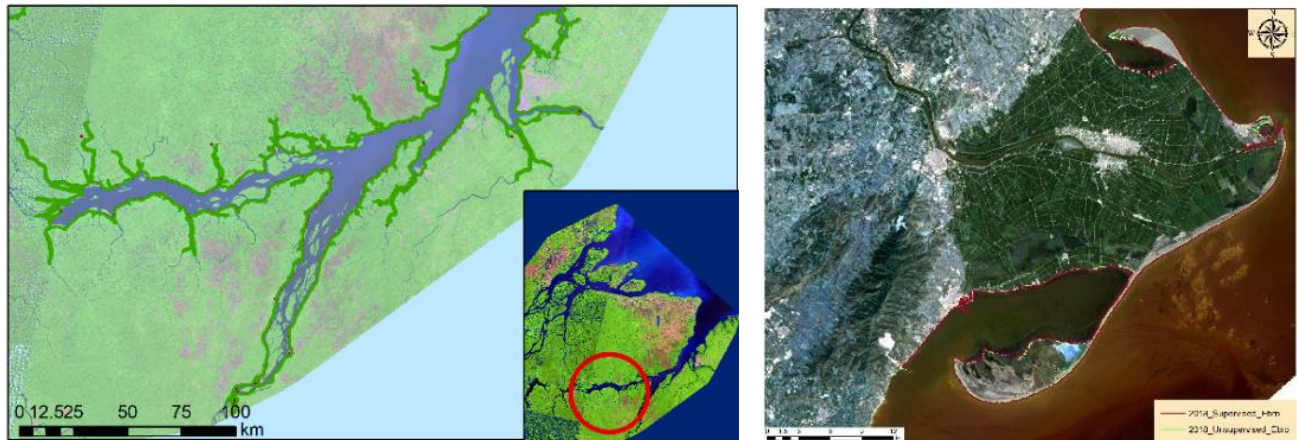


1051 where  $L_E$  is the length of the extracted shoreline,  $L_R$  is the length of the real shoreline, and  $D_{EA}$  is  
 1052 the averaged perpendicular distance between the extracted and real shoreline. The  $R$  index value  
 1053 increases as the shoreline extracted by a given method is closer to the real shoreline in length,  
 1054 whereas robustness decreases as the extracted shoreline is farther away from the real shoreline.  
 1055 Best and worst performing techniques of each delta are summarized in Figure 15 below.



1057 **Figure 15: A summary of the best and worst performing techniques of the sample deltas.**

1058 Analyses show that, except for two cases (the Po and Irrawaddy Deltas), Unsupervised and  
 1059 Supervised Classifications performed the best across all morphology indicators (e.g. beach spits,  
 1060 tombolos, shoreline) (Figure 16). For the Po and Irrawaddy Deltas, the Support Vector Machine  
 1061 algorithm performed the best. PCA ranked the lowest among the techniques for all the deltas,  
 1062 and we attribute these low PCA scores to the non-capture of boundary line land-sea pixels as  
 1063 ‘noise’, from the first few principal components during the transformation process.



1064

1065 **Figure 16: Algorithm performance on delta morphology indicators. *left*: the detailed extraction of**  
 1066 **extensive channel networks of the Amazon river subsequent to unsupervised classification. *Right*: A**  
 1067 **comparison of vectors of shoreline and beach spit extractions between unsupervised (green) and**  
 1068 **supervised (red) of the Ebro delta.**

1069 However, when the performance of all the techniques were summarized (Table 1) and analyzed  
 1070 for robustness, we find that Unsupervised Classification yielded the best performance on  
 1071 average. A nonparametric ANOVA showed that when all river deltas were considered,  
 1072 Robustness ( $R$ ) values of Unsupervised Classifications were significantly outperforming all the  
 1073 other techniques. SVM, Supervised Classifications, and Random Forest Classifications did not  
 1074 show a significant difference ( $\alpha = 0.05$ ) between each other. The two ratioing techniques'  
 1075 performance also did not have a significant difference between each other ( $P=0.79$ ;  $\alpha = 0.05$ ). All  
 1076 other techniques had significant differences with PCA (Table 1).

1077 **Table 3: The ranges of the percentage lengths of extracted shorelines, their average distances from**  
 1078 **the real shoreline and mean robustness values for each technique, for the entire suit of deltas (10)**  
 1079 **analyzed.**

1080  
1081  
1082  
1083  
1084  
1085

Technique	Range of $L_E$ (%) (Median in parenthesis)	Range of $D_{EA}$ (m) (Median in parenthesis)	R mean
Unsupervised	78-100 (98)	40-239 (45)	1.72
SVM	36-99 (79)	42-340 (60)	1.17
Supervised	56-99 (87)	45-246 (87)	1.14
Random Forest	45-97 (76)	45-471 (78)	0.95
MNDWI	23-79 (50)	78-587 (229)	0.32
NDVI	29-70 (52)	105-623 (172)	0.31
PCA	4-84 (24)	75-2668 (427)	0.19

1086  
1087  
1088  
1089  
1090  
1091  
1092  
1093  
1094  
1095  
1096  
1097  
1098  
1099

We did not observe clustering of techniques around delta types, nor between deltas in specific Köppen climate classes. However, it must be noted that these are only a small sample of deltas from each delta type and Köppen category. It was interesting to note how although past literature showed that support vector machines (SVMs) as the best among pixel-based classifications, our comparisons yield mixed outcomes (SVM performing best in only 2 cases out of the 10, and second ranked in all other cases). We attribute this to two reasons: 1) classification algorithm accuracies depend vastly on the resolution of the satellites, and 2) the training data that we used for the SVMs were derived from other satellite products (of higher resolutions than Landsat). The literature review reflects a variety of resolutions and sources as opposed to our use of 30 m Landsat imagery for all the case studies. On the other hand, some studies used in-situ field measurements as training data which likely led to higher classification accuracy. However, given the almost similar accuracies of unsupervised classification and SVM, we recommend the prior (as SVMs require good training data and takes time for algorithm development) for deltaic feature detection based on Landsat imagery.

1100  
1101

In a synergistic study, Munasinghe et al. (under review) evaluated 5 conventional remote sensing techniques (the same as used in this study) on 44 global river deltas worldwide in an attempt to

1102 infer on the performance of techniques in shoreline extraction in different types of deltas (River,  
1103 Tide, Wave-dominated) in different geographic/climatic regions. A major goal of that study was  
1104 to draw common generalizations and working behaviors of techniques around well-known types  
1105 of deltas and apply them to lesser studied, data sparse regions. Results showed that Unsupervised  
1106 classification yielded the best performance for the majority of the deltas (35 of 44) whilst  
1107 supervised classification yielded the best for the remainders (9 of 44). They also found that  
1108 extraction accuracies were higher in wave dominated deltas, lower for tide-dominated deltas, and  
1109 moderate for river-dominated deltas. Reasons were attributed to the alongshore sediment  
1110 transport processes of the wave-dominated deltas, resulting in sandy shorelines which has higher  
1111 contrast with the less-muddied ocean making it easier for land-water boundary identification. In  
1112 comparison, sediment-rich murky waters in the nearshore environment governed by the intertidal  
1113 oscillations in tide-dominated deltas provided less contrast with land. Hence reduced extraction  
1114 accuracies. Based on results of both these studies, we recommend the use of Unsupervised  
1115 Classification as a first order extraction technique for data sparse deltas or previously unstudied  
1116 deltaic regions.

## 1117 **7. Future Directions**

1118 Based on our evaluation of the literature, we see four areas which we deem most opportune for  
1119 future development:

### 1120 **Direction 1: Utilization of higher resolution imagery and developing better sub-pixel data** 1121 **mining techniques**

1122 An important aspect that we recognized earlier was that, compared to shoreline changes, there  
1123 was a dearth in the number of studies that focused on other environmental indicators of delta

1124 morphology change. This was explained by the fact that the shoreline governs the effective  
1125 landmass that is suitable for human use and is prudent to know the progradation and degradation  
1126 of a delta against sea level rise and fast changing climatic conditions. Consequently, shoreline  
1127 change studies, evidently, seem to have greater weightage and research merit than other  
1128 indicators. We, however, would like to bring out a different perspective to the problem in  
1129 recognizing that technological limitation is also an important governing factor of these disparate  
1130 numbers. Specifically, the spatial resolutions of earth observing satellites that are used to detect  
1131 environmental indicators of river delta morphology change.

1132 Detecting the shoreline of a delta, although as described earlier is quite complicated, can be  
1133 performed relatively well with imagery with moderate spatial resolution (in the range of 30 – 250  
1134 m). On the other hand, detecting crevasse splays, channel avulsions and anastomosis of channels  
1135 with a high level of accuracy, especially in smaller channels and topographically challenging  
1136 regions, require very high-resolution satellite imagery (below 10 m). The problem is exacerbated  
1137 if these changes are required to be detected in particularly small deltas, as the background noise  
1138 from surrounding, non-deltaic, features can heavily influence these analyses.

1139 In the last decade, we experienced a great increase in the availability of higher resolution satellite  
1140 imagery, primarily through commercial space programs (e.g. Planet Labs, Airbus Defense and  
1141 Space, Inc.). These sub-meter resolution platforms could be instrumental in detecting intricate  
1142 deltaic features. Striving for higher resolutions, however, comes at a cost. With an exception of  
1143 programs that provide conditional access to high resolution satellite archives (e.g. Planet labs),  
1144 most of these platforms are payment-based, and imagery acquisition could be a significant  
1145 proponent of the project budget. Costs also include data storage and purchase and maintenance  
1146 of high-powered computational systems. Due to exorbitant costs, and also due to limited archival

1147 length (since most of these platforms are new, the length of their archives is not sufficient for  
1148 delta change studies), the usage of higher resolution platforms is still limited in deltaic research.  
1149 However, it can be expected that, as time progresses, the use of these platforms will increase  
1150 dramatically.

1151 In the meantime, fusion of high and medium resolution imagery for detecting fine resolution  
1152 deltaic features is one promising way forward. Image fusion and the consequent overall increase  
1153 in resolution presents a solution to another problem: presence of mixed pixels in shoreline  
1154 classification. As described earlier, this issue has been recognized as a major problem  
1155 influencing the accuracy of remote-sensing image classification (Liu *et al.*, 2016). Theoretically,  
1156 with improvements in imagery spatial resolution, the number of mixed pixels will be greatly  
1157 decreased (Wu, 2009).

1158 There is also great potential in developing novel data mining algorithms, especially sub-pixel  
1159 algorithms (which have historically shown success in the literature) that can be used with already  
1160 existing moderate spatial resolution platforms. Examples of such algorithms, which were  
1161 recently applied to delta morphology studies, include the grid-based collocation pattern mining  
1162 technique (Sainju and Zhang, 2017), Spectral Unmixing Algorithm Based on Distance Geometry  
1163 (Pu *et al.*, 2013), and the use of colorimetry to estimate the proportion of classes in mixed pixels  
1164 (Suresh and Jain, 2018). Finding solutions to sub-pixel information will not only help advance  
1165 morphological science forward but could also provide great impetus to the studies that will be  
1166 forthcoming using high resolution satellite imagery.

1167 **Direction 2: Use of automated pattern recognition techniques, universal applicability and**  
1168 **algorithm transferability across platforms**

1169 Although there exist several manual/semi-automated methods to extract information from  
1170 satellite imagery as discussed in the sections above, we see great advantages in extraction of  
1171 information though automated techniques for change detection which could reduce the errors due  
1172 to operator bias and more efficiently partition and recognize patterns and relationships in  
1173 datasets.

1174 In this context, we think that “Smart Data Discovery - the idea of automating the identification of  
1175 patterns and trends in large data sets” (Sallam *et al.*, 2017) - can play an important role in feature  
1176 extraction from satellite big data. Smart data discovery is currently used increasingly in the  
1177 business intelligence sector in making informed market decisions (Sallam *et al.*, 2017). We think  
1178 however, that there is great potential for this technique in the domain of satellite remote sensing  
1179 to prepare and cleanse data more intelligently, automatically find hidden patterns and  
1180 correlations in data, especially where traditional and even semi-automatic machine learning  
1181 techniques are expensive, difficult and time intensive to implement.

1182 Algorithms that we develop also need to be near-universally applicable. Localized algorithms  
1183 which work perfectly in one particular region or for a particular size and type of delta often do  
1184 not perform well in other locations and is thus of relatively limited use elsewhere. To the holistic  
1185 study of Earth’s geomorphology and its evolution, continental deltaic dynamics is warranted.  
1186 There is importance of looking at how these landforms change at large scales, hence, the need for  
1187 universal techniques. Such techniques are, unfortunately, have yet to be developed.

1188 It is to be expected that the number of remote sensing application of delta morphology analysis  
1189 will increase in the near future due to continued extensions of freely-available satellite imagery  
1190 archives (e.g. Landsat, MODIS), and increased availability of higher resolution imagery via  
1191 commercial and government platforms. It is therefore important to promote algorithm  
1192 developments with the capability to be transferred across platforms (e.g. to efficiently upscale  
1193 and downscale information from different spatial resolutions). This will enhance their longevity  
1194 and utility to the entire constellation of satellites.

### 1195 **Direction 3: Improvement of Ancillary data**

1196 In our and others' view, inclusion of additional explanatory variables that can differentiate  
1197 spectral classes is more promising than enhancement of the image processing technique alone  
1198 (Khatami *et al.*, 2016). Common examples include topographic data such as digital elevation  
1199 models, slope, aspect layers, geological layers, data from active sensors such as synthetic  
1200 aperture radar or LiDAR, data from passive sensors, data from different temporal rates of  
1201 phenological changes in vegetation mapping, and anisotropy of land surface reflectance. The  
1202 inclusion of such data gives additional data layers of information that can be utilized in the  
1203 problem-solving framework (e.g. Figure 7: The additional information that contributes to the  
1204 understanding of deltaic evolution) to solve for the complexities of the deltaic environment more  
1205 easily.

1206 There exist challenges, however, in collecting ancillary data. Firstly, there is a regional disparity  
1207 in the quantity of data collected. Although data is abundantly collected and housed in most of the  
1208 economically developed countries of the world, data collection is sparse in the developing  
1209 countries. Second is the bureaucracy of organizations which own these data. The lack of open



1210 data policies makes it difficult for researchers to access them. Thirdly, the culture of data sharing  
1211 among researchers. Research culture should orient itself in a direction of openly sharing data  
1212 subsequent to your own research for other interested parties to build up on. This culture is  
1213 gathering momentum through public platforms like GitHub, researchgate, HydroShare, and stack  
1214 exchanges. We however, envision the need of more subject-specific research repositories.

#### 1215 **Direction 4: A Global Information System of deltaic data**

1216 One of the major challenges for researchers working in the domain of deltaic remote sensing is  
1217 that there is a lack of ground truth data to validate their observations against. On the other hand,  
1218 field geomorphologists, who base their research efforts on identifying changes in deltaic features  
1219 on a local scale, would immensely benefit from the “bigger picture” of the deltaic domain from  
1220 the remote sensing community. One of the major challenges has been to build a data sharing  
1221 bridge between these two communities. There currently exists no portal/database/repository  
1222 which offers different types of data in relation to deltaic research. A repository for river deltaic  
1223 research similar to, for example, HydroShare should be established. HydroShare (Tarboton *et al.*,  
1224 2014), operated by the Consortium of Universities for the Advancement of Hydrologic Science,  
1225 Inc. (CUAHSI), is an online collaboration environment for sharing data, models, and code  
1226 related to hydrology. A delta repository could (conceptually) include field data (e.g. soil types,  
1227 point climate data, different land use types) collected by field researchers, remotely sensed data  
1228 (e.g. locations and extents of deltaic features, land use class delineations, temporal change of  
1229 features), different numerical models which model deltaic features (e.g. crevasse splays,  
1230 avulsions, shoreline changes), and publicly volunteered and vetted geographic information. We  
1231 believe that such a repository will foster collaborative and interdisciplinary research and help to  
1232 propel deltaic research to the next level.

## 1233 **8. Conclusions**

1234 River deltas are important landforms that serve many societal and ecological functions.

1235 Assessing changes to delta morphology is important to identify vulnerable areas and sustainably  
1236 manage deltaic land. Satellite remote sensing provides an effective way of detecting delta  
1237 morphology change over time.

1238 This review focused on Remote Sensing Techniques that are used in detecting delta morphology  
1239 change. We discussed 18 such techniques, their strengths and their caveats with regard to deltaic  
1240 feature extraction and change detection. Review of literature suggests that sub-pixel algorithms  
1241 such as spectral mixture analysis and Fuzzy logic yield very high accuracies, while machine  
1242 learning techniques ranked second. Support Vector Machines rank as the best individual machine  
1243 learning technique across reviewed literature. We also found that the use of an ensemble of  
1244 techniques (a machine learning technique ensemble, or a mix of machine learning and  
1245 conventional ones) yield high accuracies.

1246 The choice of the technique(s) that one should preferably use to extract features of a river delta is  
1247 governed primarily by the complexity of the delta. Simple deltas can be analyzed using relatively  
1248 simple techniques and vice versa. We also found that the choice of technique depends on how  
1249 data intensive the algorithm is, the availability of resources (time and computational resource),  
1250 and the skill level of the user (e.g. machine learning applications requires specific skillsets). A  
1251 comparison study performed between 10 deltas using 7 algorithms yielded unsupervised  
1252 classification as the go-to method for quick and robust delta-morphology-indicator detection.

1253 We discuss the pathway forward for future research by recognizing the utility of using different  
1254 delta morphology remote sensing techniques on one particular river delta to gain a better

1255 understanding of its landmass evolution, and also of the importance of comparison studies across  
1256 deltas to infer on the similarities/dissimilarities of morphological changes and identify strengths  
1257 limitations of remote sensing techniques themselves in different geographic/climatic conditions.  
1258 Four directions in which how future research will benefit are presented. The importance of  
1259 higher spatial resolutions and the need for the development of more robust sub-pixel detection  
1260 algorithms to mine data from moderate resolution imagery to more accurately infer on deltaic  
1261 features such as smaller channel avulsions and formation of splays, is highlighted. The  
1262 importance of automated pattern recognition techniques, universal applicability of algorithms,  
1263 and algorithm-transferability across platforms are discussed. Thirdly, the effective use of  
1264 ancillary data to make better judgement calls during the deltaic feature extraction process are  
1265 brought forth, and finally, the concept of a repository which houses different types of data and  
1266 models pertaining to deltaic research which is envisioned to foster interdisciplinary collaboration  
1267 are opined.

## 1268 **9. References**

- 1269 Adams, J.B., Sabol, D.E., Kapos, V., Almeida Filho, R., Roberts, D.A., Smith, M.O., Gillespie,  
1270 A.R., 1995. Classification of multispectral images based on fractions of endmembers:  
1271 Application to land-cover change in the Brazilian Amazon. *Remote sensing of Environment*,  
1272 52(2), 137-154. [https://doi.org/10.1016/0034-4257\(94\)00098-8](https://doi.org/10.1016/0034-4257(94)00098-8)
- 1273 Adam, E M., Mutanga, O., Rugege, D., Ismail, R., 2012. Discriminating the papyrus vegetation  
1274 (*Cyperus papyrus* L.) and its co-existent species using random forest and hyperspectral data  
1275 resampled to HYMAP. *International Journal of Remote Sensing*, 33(2), 552-569.  
1276 <https://doi.org/10.1080/01431161.2010.543182>
- 1277 Adegoke, J.O., Fageja, M., James, G., Agbaje, G., Ologunorisa, T.E., 2010. An assessment of  
1278 recent changes in the Niger Delta coastline using satellite imagery. *Journal of Sustainable*  
1279 *Development*, 3(4), 277. <https://doi.org/10.5539/jsd.v3n4p277>
- 1280 Ahmed, A., Drake, F., Nawaz, R., Woulds, C., 2018. Where is the coast? Monitoring coastal land  
1281 dynamics in Bangladesh: An integrated management approach using GIS and remote sensing

- 1282 techniques. *Ocean & Coastal Management*, 151, 10-24.  
1283 <https://doi.org/10.1016/j.ocecoaman.2017.10.030>
- 1284 Akar, Ö., and Güngör, O., 2015. Integrating Multiple Texture Methods and NDVI to the Random  
1285 Forest Classification Algorithm to Detect Tea and Hazelnut Plantation Areas in Northeast  
1286 Turkey. *International Journal of Remote Sensing* 36(2): 442–464.  
1287 <https://doi.org/10.1080/01431161.2014.995276>
- 1288 Alesheikh, A.A., Ghorbanali, A., Nouri, N., 2007. Coastline change detection using remote  
1289 sensing. *International Journal of Environmental Science & Technology*, 4(1), 61-66.  
1290 <https://doi.org/10.1007/BF03325962>
- 1291 Al Fugura, A., Billa, L., Pradhan, B., 2011. Semi-automated procedures for shoreline extraction  
1292 using single RADARSAT-1 SAR image. *Estuarine, Coastal and Shelf Science*, 95(4), 395-400.  
1293 <https://doi.org/10.1016/j.ecss.2011.10.009>
- 1294 Allen, Y. C., Couvillion, B. R., Barras, J. A., 2012. Using multitemporal remote sensing imagery  
1295 and inundation measures to improve land change estimates in coastal wetlands. *Estuaries and*  
1296 *Coasts*, 35(1), 190-200. <https://doi.org/10.1007/s12237-011-9437-z>
- 1297 Allison, M.A., Khan, S.R., Goodbred Jr, S.L., Kuehl, S.A., 2003. Stratigraphic evolution of the  
1298 late Holocene Ganges–Brahmaputra lower delta plain. *Sedimentary Geology*, 155(3-4), 317-342.  
1299 [https://doi.org/10.1016/S0037-0738\(02\)00185-9](https://doi.org/10.1016/S0037-0738(02)00185-9)
- 1300 Banks, S., Millard, K., Pasher, J., Richardson, M., Wang, H., Duffe, J., 2015. Assessing the  
1301 potential to operationalize shoreline sensitivity mapping: Classifying multiple Wide Fine  
1302 Quadrature Polarized RADARSAT-2 and Landsat 5 scenes with a single Random Forest model.  
1303 *Remote Sensing*, 7(10), 13528-13563. <https://doi.org/10.3390/rs71013528>
- 1304 Bayarjargal, Y., Karnieli, A., Bayasgalan, M., Khudulmur, S., Gandush, C., Tucker, C.J., 2006.  
1305 A comparative study of NOAA–AVHRR derived drought indices using change vector analysis.  
1306 *Remote Sensing of Environment*, 105(1), 9-22. <https://doi.org/10.1016/j.rse.2006.06.003>
- 1307 Bayram, B., Acar, U., Seker, D., Ari, A., 2008. A novel algorithm for coastline fitting through a  
1308 case study over the Bosphorus. *Journal of Coastal Research*, 983-991. <https://doi.org/10.2112/07-0825.1>
- 1310 Bendsen, H., Meyer, T., 2002. The dynamics of land use systems in Ngamiland: Changing  
1311 livelihood options and strategies. In: *Environmental Monitoring of Tropical Wetlands*,  
1312 *Proceedings of a Wetland Conference*, Maun, Botswana (pp. 278-304).
- 1313 Berberoglu, S., Lloyd, C.D., Atkinson, P.M., Curran, P.J., 2000. The integration of spectral and  
1314 textural information using neural networks for land cover mapping in the Mediterranean.  
1315 *Computers & Geosciences*, 26(4), 385-396. [https://doi.org/10.1016/S0098-3004\(99\)00119-3](https://doi.org/10.1016/S0098-3004(99)00119-3)
- 1316 Berhane, T., Lane, C., Wu, Q., Autrey, B., Anenkhonov, O., Chepinoga, V., Liu, H., 2018.  
1317 Decision-tree, rule-based, and random forest classification of high-resolution multispectral

- 1318 imagery for wetland mapping and inventory. *Remote sensing*, 10(4), 580.  
1319 <https://doi.org/10.3390/rs10040580>
- 1320 Blaschke, T., 2010. Object based image analysis for remote sensing. *ISPRS Journal of*  
1321 *Photogrammetry and Remote Sensing*, 65(1), 2–16.  
1322 <https://doi.org/10.1016/j.isprsjprs.2009.06.004>
- 1323 Braud, D.H., Feng, W., 1998. Semi-automated construction of the Louisiana coastline digital  
1324 land/water boundary using Landsat Thematic Mapper satellite imagery (Department of  
1325 Geography and Anthropology, Louisiana State University, Louisiana Applied Oil Spill Research  
1326 and Development Program), OSRAPD Technical Report. 97-002.
- 1327 Breiman, L., 2001. Random forests. *Machine learning*, 45(1), 5-32.  
1328 <https://doi.org/10.1023/A:1010933404324>
- 1329 Buono, A., Nunziata, F., Migliaccio, M., Yang, X., Li, X., 2017. Classification of the Yellow  
1330 River delta area using fully polarimetric SAR measurements. *International journal of remote*  
1331 *sensing*, 38(23), 6714-6734. <https://doi.org/10.1080/01431161.2017.1363437>
- 1332 Cao, M., Liu, G., Zhang, X., 2007. An object-oriented approach to map wetland vegetation: a  
1333 case study of yellow river delta. In 2007 IEEE International Geoscience and Remote Sensing  
1334 Symposium. pp 4585-4587.
- 1335 Chen, J., Gong, P., He, C., Pu, R., Shi, P., 2003. Land-use/land-cover change detection using  
1336 improved change-vector analysis. *Photogrammetric Engineering & Remote Sensing*, 69(4), 369-  
1337 379. <https://doi.org/10.14358/PERS.69.4.369>
- 1338 Chen, C., Fu, J., Zhang, S., Zhao, X., 2019. Coastline information extraction based on the  
1339 tasseled cap transformation of Landsat-8 OLI images. *Estuarine, Coastal and Shelf Science*, 217,  
1340 281-291. <https://doi.org/10.1016/j.ecss.2018.10.021>
- 1341 Chu, Z.X., Sun, X.G., Zhai, S.K., Xu, K.H., 2006. Changing pattern of accretion/erosion of the  
1342 modern Yellow River (Huanghe) subaerial delta, China: Based on remote sensing images.  
1343 *Marine Geology*, 227(1-2), 13-30. <https://doi.org/10.1016/j.margeo.2005.11.013>
- 1344 Ciavola, P., 1999. Relation between river dynamics and coastal changes in Albania: an  
1345 assessment integrating satellite imagery with historical data. *International Journal of Remote*  
1346 *Sensing*, 20(3), 561-584. <https://doi.org/10.1080/014311699213343>
- 1347 Civco, D.L., Hurd, J.D., Wilson, E.H., Song, M., Zhang, Z., 2002. A comparison of land use and  
1348 land cover change detection methods. In ASPRS-ACSM Annual Conference (Vol. 21).
- 1349 Cohen, W.B., Fiorella, M., Gray, J., Helmer, E., Anderson, K., 1998. An efficient and accurate  
1350 method for mapping forest clearcuts in the Pacific Northwest using Landsat imagery.  
1351 *Photogrammetric Engineering and Remote Sensing*, 64(4), 293-299.
- 1352 Coleman, J.M., Wright, L.D., 1975. Modern river deltas: variability of processes and sand  
1353 bodies. In: Broussard M.L., *Deltas: models for Exploration*. Houston Geological Society. pp. 99-  
1354 149.

- 1355 Congalton, R.G., 1991. A review of assessing the accuracy of classifications of remotely sensed  
1356 data. *Remote sensing of environment*, 37(1), 35-46.
- 1357 Crist, E.P., 1985. A TM tasseled cap equivalent transformation for reflectance factor data.  
1358 *Remote Sensing of Environment*, 17(3), 301-306.
- 1359 Cui, B. L., Li, X. Y., 2011. Coastline change of the Yellow River estuary and its response to the  
1360 sediment and runoff (1976–2005). *Geomorphology*, 127(1-2), 32-40.  
1361 <https://doi.org/10.1016/j.geomorph.2010.12.001>
- 1362 Dada, O. A., Li, G., Qiao, L., Asiwaju-Bello, Y. A., Anifowose, A. Y. B., 2018. Recent Niger  
1363 Delta shoreline response to Niger River hydrology: Conflict between forces of Nature and  
1364 Humans. *Journal of African Earth Sciences*, 139, 222-231.  
1365 <https://doi.org/10.1016/j.jafrearsci.2017.12.023>
- 1366 Da Silva, A. G. A., Stattegger, K., Vital, H., & Schwarzer, K. (2019). Coastline change and  
1367 offshore suspended sediment dynamics in a naturally developing delta (Parnaíba Delta, NE  
1368 Brazil). *Marine Geology*, 410, 1-15. <https://doi.org/10.1016/j.margeo.2018.12.013>
- 1369 Del Frate, F., Latini, D., Minchella, A., Palazzo, F., 2012. A new automatic technique for  
1370 coastline extraction from SAR images. In: *SAR Image Analysis, Modeling, and Techniques XII*  
1371 (Vol. 8536, p. 85360R). International Society for Optics and Photonics.
- 1372 Dellepiane, S., De Laurentiis, R., Giordano, F., 2004. Coastline extraction from SAR images and  
1373 a method for the evaluation of the coastline precision. *Pattern Recognition Letters*, 25(13), 1461-  
1374 1470. <https://doi.org/10.1016/j.patrec.2004.05.022>
- 1375 Demers, A.M., Banks, S.N., Pasher, J., Duffe, J., Laforest, S., 2015. A comparative analysis of  
1376 object-based and pixel-based classification of RADARSAT-2 C-band and optical satellite data  
1377 for mapping shoreline types in the Canadian arctic. *Canadian Journal of Remote Sensing*, 41(1),  
1378 1-19. <https://doi.org/10.1080/07038992.2015.1020361>
- 1379 Deng, J.S., Wang, K., Deng, Y.H., Qi, G.J., 2008. PCA-based land-use change detection and  
1380 analysis using multitemporal and multisensor satellite data. *International Journal of Remote*  
1381 *Sensing*, 29(16), 4823-4838. <https://doi.org/10.1080/01431160801950162>  
1382
- 1383 Denison, D.G., Mallick, B.K., Smith, A.F., 1998. A bayesian CART algorithm. *Biometrika*,  
1384 85(2), 363-377. <https://doi.org/10.1093/biomet/85.2.363>
- 1385 Dewi, R., Bijker, W., Stein, A., Marfai, M., 2016. Fuzzy classification for shoreline change  
1386 monitoring in a part of the northern coastal area of Java, Indonesia. *Remote sensing*, 8(3), 190.  
1387 <https://doi.org/10.3390/rs8030190>
- 1388 Ding, W.J., Wang, R.Q., Wu, D.Q., Liu, J., 2013. Cellular automata model as an intuitive  
1389 approach to simulate complex land-use changes: an evaluation of two multi-state land-use  
1390 models in the Yellow River Delta. *Stochastic Environmental Research and Risk Assessment*,  
1391 27(4), 899-907. <https://doi.org/10.1007/s00477-012-0624-7>

- 1392 Ekercin, S., 2007. Coastline change assessment at the Aegean Sea coasts in Turkey using  
1393 multitemporal Landsat imagery. *Journal of Coastal Research*, 691-698.  
1394 <https://doi.org/10.2112/04-0398.1>
- 1395 El-Asmar, H.M., Hereher, M.E., 2011. Change detection of the coastal zone east of the Nile  
1396 Delta using remote sensing. *Environmental Earth Sciences*, 62(4), 769-777.  
1397 <https://doi.org/10.1007/s12665-010-0564-9>
- 1398 Elhag, M., Psilovikos, A., Sakellariou-Makrantonaki, M., 2013. Land use changes and its  
1399 impacts on water resources in Nile Delta region using remote sensing techniques. *Environment,*  
1400 *Development and Sustainability*, 15(5), 1189-1204. <https://doi.org/10.1007/s10668-013-9433-5>
- 1401 El-Kawya, O.A., Rød, J.K., Ismail, H.A., Suliman, A.S., 2011. Land use and land cover change  
1402 detection in the western Nile delta of Egypt using remote sensing data. *Applied Geography*,  
1403 31(2), 483-494. <https://doi.org/10.1016/j.apgeog.2010.10.012>
- 1404 El Raey, M., Nasr, S.M., Frihy, O.E., El Hattab, M.M., 1995. Change detection of Rosetta  
1405 promontory over the last forty years. *International Journal of Remote Sensing*, 16, 825-834  
1406 <https://doi.org/10.1080/01431169508954446>
- 1407 El-Raey, M., El-Din, S.S., Khafagy, A.A., Abo Zed, A.I., 1999. Remote sensing of beach  
1408 erosion/accretion patterns along Damietta-Port Said shoreline, Egypt. *International Journal of*  
1409 *Remote Sensing*, 20(6), 1087-1106. <https://doi.org/10.1080/014311699212867>
- 1410 Elliott T., 1986. Deltas. In: Reading H.G. (Ed.) *Sedimentary Environments and Facies*,  
1411 Blackwell Scientific Publications, Oxford, pp. 113-154.
- 1412 Enderle, D.I., Weih Jr, R.C., 2005. Integrating supervised and unsupervised classification  
1413 methods to develop a more accurate land cover classification. *Journal of the Arkansas Academy*  
1414 *of Science*, 59(1), 65-73.
- 1415 Foody, G.M., McCulloch, M.B., Yates, W.B., 1995. Classification of Remotely Sensed Data by  
1416 an Artificial Neural Network: Issues Related to Training Data. *Photogrammetric Engineering &*  
1417 *Remote Sensing*, 61(4), 391-401.
- 1418 Foody, G.M., Mathur, A., 2006. The use of small training sets containing mixed pixels for  
1419 accurate hard image classification: Training on mixed spectral responses for classification by a  
1420 SVM. *Remote sensing of Environment*, 103(2), 179-189.  
1421 <https://doi.org/10.1016/j.rse.2006.04.001>
- 1422 Foody, G.M., Muslim, A.M., Atkinson, P.M., 2005. Super-resolution mapping of the waterline  
1423 from remotely sensed data. *International Journal of Remote Sensing*, 26(24), 5381-5392.  
1424 <https://doi.org/10.1080/01431160500213292>
- 1425 Frazier, P.S., Page, K.J., 2000. Water body detection and delineation with Landsat TM data,  
1426 *Photogrammetric Engineering & Remote Sensing*, 66 (2), 1461-1467.

- 1427 Friedl, M.A., Brodley, C.E., 1997. Decision tree classification of land cover from remotely  
1428 sensed data. *Remote sensing of Environment*, 61(3), 399-409. [https://doi.org/10.1016/S0034-](https://doi.org/10.1016/S0034-4257(97)00049-7)  
1429 [4257\(97\)00049-7](https://doi.org/10.1016/S0034-4257(97)00049-7)
- 1430 Frihy, O.E., Dewidar, K.M., Nasr, S.M., El Raey, M.M., 1998. Change detection of the  
1431 northeastern Nile Delta of Egypt: shoreline changes, Spit evolution, margin changes of Manzala  
1432 lagoon and its islands. *International Journal of Remote Sensing*, 19(10), 1901-1912.  
1433 <https://doi.org/10.1080/014311698215054>
- 1434 Frohn, R.C., D'Amico, E., Lane, C., Autrey, B., Rhodus, J., Liu, H., 2012. Multi-temporal sub-  
1435 pixel Landsat ETM+ classification of isolated wetlands in Cuyahoga County, Ohio, USA.  
1436 *Wetlands*, 32(2), 289-299. <https://doi.org/10.1007/s13157-011-0254-8>
- 1437 Ghanavati, E., Firouzabadi, P.Z., Jangi, A.A., Khosravi, S., 2008. Monitoring geomorphologic  
1438 changes using Landsat TM and ETM+ data in the Hendijan River delta, southwest Iran.  
1439 *International Journal of Remote Sensing*, 29(4), 945-959.  
1440 <https://doi.org/10.1080/01431160701294679>
- 1441 Ghoneim, E., Mashaly, J., Gamble, D., Halls, J., AbuBakr, M., 2015. Nile Delta exhibited a  
1442 spatial reversal in the rates of shoreline retreat on the Rosetta promontory comparing pre-and  
1443 post-beach protection. *Geomorphology*, 228, 1-14.  
1444 <https://doi.org/10.1016/j.geomorph.2014.08.021>
- 1445 Gislason, P.O., Benediktsson, J.A., Sveinsson, J.R., 2006. Random forests for land cover  
1446 classification. *Pattern Recognition Letters*, 27(4), 294-300.  
1447 <https://doi.org/10.1016/j.patrec.2005.08.011>
- 1448 Gong, P., 1993. Change detection using Principal Component Analysis and Fuzzy set theory.  
1449 *Canadian Journal of Remote Sensing*, 19(1), 22-29.  
1450 <https://doi.org/10.1080/07038992.1993.10855147>
- 1451 Gopinath, G., Seralathan, P., 2005. Rapid erosion of the coast of Sagar island, West Bengal-  
1452 India. *Environmental Geology*, 48(8), 1058-1067. <https://doi.org/10.1007/s00254-005-0044-9>
- 1453 Gou, S., Li, X., Yang, X., 2016. Coastal zone classification with fully polarimetric SAR imagery.  
1454 *IEEE Geoscience and Remote Sensing Letters*, 13(11), 1616-1620.  
1455 <https://doi.org/10.1109/LGRS.2016.2597965>
- 1456 Guariglia, A., Buonamassa, A., Losurdo, A., Saladino, R., Trivigno, M.L., Zaccagnino, A.,  
1457 Colangelo, A., 2006. A multisource approach for coastline mapping and identification of  
1458 shoreline changes. *Annals of geophysics*, 49(1).
- 1459 Gugliotta, M., Saito, Y., 2019. Matching trends in channel width, sinuosity, and depth along the  
1460 fluvial to marine transition zone of tide-dominated river deltas: The need for a revision of  
1461 depositional and hydraulic models. *Earth-science reviews*.  
1462 <https://doi.org/10.1016/j.earscirev.2019.02.002>



- 1463 Gutierrez, B.T., Plant, N.G., Thieler, E.R., 2011. A Bayesian network to predict coastal  
1464 vulnerability to sea level rise. *Journal of Geophysical Research: Earth Surface*, 116(F2).  
1465 <https://doi.org/10.1029/2010JF001891>
- 1466 Haas, J., Ban, Y., 2014. Urban growth and environmental impacts in Jing-Jin-Ji, the Yangtze,  
1467 River Delta and the Pearl River Delta. *International Journal of Applied Earth Observation and*  
1468 *Geoinformation*, 30, 42-55. <https://doi.org/10.1016/j.jag.2013.12.012>
- 1469 Heimann, T., Thorn, M., Kunert, T., Meinzer, H.P., 2004. New methods for leak detection and  
1470 contour correction in seeded region growing segmentation. In 20th ISPRS Congress, Istanbul  
1471 (Vol. 35, pp. 317-322).
- 1472 Heumann, B.W., 2011. An object-based classification of mangroves using a hybrid decision  
1473 tree—Support vector machine approach. *Remote Sensing*, 3(11), 2440-2460.  
1474 <https://doi.org/10.3390/rs3112440>
- 1475 Huang, Z., Lees, B.G., 2004. Combining non-parametric models for multisource predictive forest  
1476 mapping. *Photogrammetric Engineering and Remote Sensing*, 70(4), pp. 415–425.  
1477 <https://doi.org/10.14358/PERS.70.4.415>
- 1478 Hutchings, R.M., Campbell, S.K., 2005. The Importance of Deltaic Wetland Resources: A  
1479 Perspective from the Nooksack River Delta, Washington State. *Journal of Wetland Archaeology*,  
1480 5(1): 17-34. <https://doi.org/10.1179/jwa.2005.5.1.17>
- 1481 Isikdogan, F., Bovik, A., Passalacqua, P., 2015. Automatic channel network extraction from  
1482 remotely sensed images by singularity analysis. *IEEE Geoscience and Remote Sensing Letters*,  
1483 12(11), 2218-2221. <https://doi.org/10.1109/LGRS.2015.2458898>
- 1484 Jarvis, C.H., Stuart, N., 1996. The sensitivity of a neural network for classifying remotely sensed  
1485 imagery. *Computers & Geosciences*, 22(9), 959-967. [https://doi.org/10.1016/S0098-  
1486 3004\(96\)00034-9](https://doi.org/10.1016/S0098-3004(96)00034-9)
- 1487 Jensen, J.R., 1996. *Introductory Digital Image Processing: A Remote Sensing Perspective*, 2<sup>nd</sup>  
1488 Edition, Englewood Cliffs, NJ: Prentice-Hall.
- 1489 Kamal, M., Phinn, S., 2011. Hyperspectral data for mangrove species mapping: A comparison of  
1490 pixel-based and object-based approach. *Remote Sensing*, 3(10), 2222–2242.  
1491 <https://doi.org/10.3390/rs3102222>
- 1492 Kelley, G.W., Hobgood, J.S., Bedford, K.W., Schwab D.J., 1998. Generation of three-  
1493 dimensional lake model forecasts for Lake Erie, *Weather and Forecasting*, 13(3), 305-315.  
1494 [https://doi.org/10.1175/1520-0434\(1998\)013<0659:GOTDLM>2.0.CO;2](https://doi.org/10.1175/1520-0434(1998)013<0659:GOTDLM>2.0.CO;2)
- 1495 Khatami, R., Mountrakis, G., Stehman, S.V., 2016. A meta-analysis of remote sensing research  
1496 on supervised pixel-based land-cover image classification processes: General guidelines for  
1497 practitioners and future research. *Remote Sensing of Environment*, 177, 89-100.  
1498 <https://doi.org/10.1016/j.rse.2016.02.028>

1499 Kim, M., Warner, T.A., Madden, M., Atkinson, D.S., 2011. Multi-scale GEOBIA with very high  
1500 spatial resolution digital aerial imagery: Scale, texture and image objects. *International Journal of*  
1501 *Remote Sensing*, 32(10), 2825–2850. <https://doi.org/10.1080/01431161003745608>

1502 Kong, D., Miao, C., Borthwick, A.G., Duan, Q., Liu, H., Sun, Q., Ye, A., Di, Z., Gong, W.,  
1503 2015. Evolution of the Yellow River Delta and its relationship with runoff and sediment load  
1504 from 1983 to 2011. *Journal of Hydrology*, 520, 157-167.  
1505 <https://doi.org/10.1016/j.jhydrol.2014.09.038>

1506 Krause, G., Bock, M., Weiers, S., Braun, G., 2004. Mapping land-cover and mangrove structures  
1507 with remote sensing techniques: A contribution to a synoptic GIS in support of coastal  
1508 management in North Brazil. *Environ. Manage.*, 34(3), 429–440. <https://doi.org/10.1007/s00267-004-0003-3>

1510 Kuenzer, C., van Beijma, S., Gessner, U., Dech, S., 2014. Land surface dynamics and  
1511 environmental challenges of the Niger Delta, Africa: Remote sensing-based analyses spanning  
1512 three decades (1986–2013). *Applied Geography*, 53, 354-368.  
1513 <https://doi.org/10.1016/j.apgeog.2014.07.002>

1514 Kuleli, T., 2010. Quantitative analysis of shoreline changes at the Mediterranean Coast in  
1515 Turkey. *Environmental monitoring and assessment*, 167(1-4), 387-397.  
1516 <https://doi.org/10.1007/s10661-009-1057-8>

1517 Kundu, S., Mondal, A., Khare, D., Mishra, P.K., Shukla, R., 2014. Shifting shoreline of Sagar  
1518 Island Delta, India. *Journal of maps*, 10(4), 612-619.  
1519 <https://doi.org/10.1080/17445647.2014.922131>

1520 Kushwaha, S.P.S., Dwivedi, R.S., Rao, B.R.M., 2000. Evaluation of various digital image  
1521 processing techniques for detection of coastal wetlands using ERS-1 SAR data. *International*  
1522 *Journal of Remote Sensing*, 21(3), 565-579. <https://doi.org/10.1080/014311600210759>

1523 Le, M. H., Hitoshi, T., Nguyen, T. T., Nguyen, T.V., 2006. Prediction of river bank erosion in  
1524 the lower Mekong river delta. In *Vietnam-Japan Estuary workshop*, Hanoi, Vietnam. pp. 22-24.

1525 Le Moigne, J., Tilton, J.C., 1995. Refining image segmentation by integration of edge and region  
1526 data. *IEEE Transactions on Geoscience and Remote Sensing*, 33(3), 605-615.  
1527 <https://doi.org/10.1109/36.387576>

1528 Le, T.V.H., Nguyen, H. N., Wolanski, E., Tran, T.C., Haruyama, S., 2007. The combined impact  
1529 on the flooding in Vietnam's Mekong River delta of local man-made structures, sea level rise,  
1530 and dams upstream in the river catchment. *Estuarine, Coastal and Shelf Science*, 71(1-2), 110-  
1531 116. <https://doi.org/10.1016/j.ecss.2006.08.021>

1532 Lee, K.S., Kim, T.H., Yun, Y.S., Shin, S.M., 2001. Spectral characteristics of shallow turbid  
1533 water near the shoreline on inter-tidal flat. *Korean Journal of Remote Sensing*, 17(2), 131–139.

1534 Lee, J. S., Jurkevich, I., 1990. Coastline detection and tracing in SAR images. *IEEE Transactions*  
1535 *on Geoscience and Remote Sensing*, 28(4), 662-668. <https://doi.org/10.1109/TGRS.1990.572976>

- 1536 Lentz, E. E., Thieler, E.R., Plant, N.G., Stippa, S.R., Horton, R.M., Gesch, D.B., 2016.  
1537 Evaluation of dynamic coastal response to sea-level rise modifies inundation likelihood. *Nature*  
1538 *Climate Change*, 6(7), 696. <https://doi.org/10.1038/nclimate2957>
- 1539 Li, H.T., Gu, H.Y., Han, Y.S., Yang, J., 2010. Object-oriented classification of high-resolution  
1540 remote sensing imagery based on an improved colour structure code and a support vector  
1541 machine. *International Journal of Remote Sensing*, 31(6), 1453-1470.  
1542 <https://doi.org/10.1080/01431160903475266>
- 1543 Li, J., Donselaar, M. E., Aria, S.E.H., Koenders, R., Oyen, A.M., 2014. Landsat imagery-based  
1544 visualization of the geomorphological development at the terminus of a dryland river system.  
1545 *Quaternary international*, 352, 100-110. <https://doi.org/10.1016/j.quaint.2014.06.041>
- 1546 Li, J., Bristow, C.S., 2015. Crevasse splay morphodynamics in a dryland river terminus: Río  
1547 Colorado in Salar de Uyuni Bolivia. *Quaternary International*, 377, 71-82.  
1548 <https://doi.org/10.1016/j.quaint.2014.11.066>
- 1549 Li, X., Yeh, A.G.O., 1998. Principal component analysis of stacked multi-temporal images for  
1550 the monitoring of rapid urban expansion in the Pearl River Delta. *International Journal of*  
1551 *Remote Sensing*, 19(8), 1501-1518. <https://doi.org/10.1080/014311698215315>
- 1552 Li, X., Yeh, A. G. O., 2004. Analyzing spatial restructuring of land use patterns in a fast growing  
1553 region using remote sensing and GIS. *Landscape and Urban planning*, 69(4), 335-354.  
1554 <https://doi.org/10.1016/j.landurbplan.2003.10.033>
- 1555 Liu, G., Zhang, L., Zhang, Q., Musyimi, Z., Jiang, Q., 2014. Spatio-temporal dynamics of  
1556 wetland landscape patterns based on remote sensing in Yellow River Delta, China. *Wetlands*,  
1557 34(4), 787-801. <https://doi.org/10.1007/s13157-014-0542-1>
- 1558 Liu, J., Feng, Q., Gong, J., Zhou, J., Li, Y., 2016. Land-cover classification of the Yellow River  
1559 Delta wetland based on multiple end-member spectral mixture analysis and a Random Forest  
1560 classifier. *International Journal of Remote Sensing*, 37(8), 1845-1867.  
1561 <https://doi.org/10.1080/01431161.2016.1165888>
- 1562 Liu, X., Deng, R., Xu, J., Zhang, F., 2017. Coupling the modified linear spectral mixture analysis  
1563 and pixel-swapping methods for improving subpixel water mapping: Application to the Pearl  
1564 River Delta, China. *Water*, 9(9), 658. <https://doi.org/10.3390/w9090658>
- 1565 Lohani B., Mason D.C., 1999. Construction of a digital elevation model of the Holderness Coast  
1566 using the waterline method and Air-borne Thematic Mapper data. *International Journal of*  
1567 *Remote Sensing*, 20(3): 593–607 <https://doi.org/10.1080/014311699213361>
- 1568 Lodhi, M.A., Rundquist, D.C., Han, L., Juzila, M.S., 1997. The potential for remote sensing of  
1569 loess soils suspended in surface water. *Journal of the American Water Resources Association*,  
1570 33(1), 111–127. <https://doi.org/10.1111/j.1752-1688.1997.tb04087.x>

1571 Loos, E.A., Niemann, K.O., 2002. Shoreline feature extraction from remotely sensed imagery.  
1572 In: International Geoscience and remote sensing symposium, 2002. IEEE Int. 6 (24–28), 3417–  
1573 3419. <https://doi.org/10.1109/IGARSS.2002.1027201>

1574 Louati, M., Saïdi, H., Zargouni, F., 2015. Shoreline change assessment using remote sensing and  
1575 GIS techniques: a case study of the Medjerda delta coast, Tunisia. *Arabian Journal of*  
1576 *Geosciences*, 8(6), 4239-4255. <https://doi.org/10.1007/s12517-014-1472-1>

1577 Lu, D., Moran, E., Batistella, M., 2003. Linear mixture model applied to Amazonian vegetation  
1578 classification. *Remote Sensing of Environment*, 87(4), 456–469.  
1579 <https://doi.org/10.1016/j.rse.2002.06.001>

1580 Lu, D., Mausel, P., Batistella, M., Moran, E., 2004. Comparison of land-cover classification  
1581 methods in the Brazilian Amazon Basin. *Photogrammetric Engineering and Remote Sensing*,  
1582 70(6), 723–731. <https://doi.org/10.14358/PERS.70.6.723>

1583 Maiti, S., Bhattacharya, A.K., 2009. Shoreline change analysis and its application to prediction:  
1584 A remote sensing and statistics based approach. *Marine Geology*, 257(1-4), 11-23.  
1585 <https://doi.org/10.1016/j.margeo.2008.10.006>

1586 Mallinis, G., Emmanoloudis, D., Giannakopoulos, V., Maris, F., Koutsias, N., 2011. Mapping  
1587 and interpreting historical land cover/land use changes in a Natura 2000 site using earth  
1588 observational data: the case of Nestos delta, Greece. *Applied Geography*, 31(1), 312-320.  
1589 <https://doi.org/10.1016/j.apgeog.2010.07.002>

1590 Malthus, T.J., Mumby, P.J., 2003. Remote sensing of the coastal zone: an overview and priorities  
1591 for future research. *International Journal of Remote Sensing*, 24, 2805–2815.  
1592 <https://doi.org/10.1080/0143116031000066954>

1593 Manavalan, P., Sathyanath, P., Rajegowda, G. L., 1993. Digital image analysis techniques to  
1594 estimate waterspread for capacity evaluations of reservoirs. *Photogrammetric Engineering and*  
1595 *Remote Sensing*, 59(9), 1389–1395.

1596 Marghany, M., Sabu, Z., Hashim, M., 2010. Mapping coastal geomorphology changes using  
1597 synthetic aperture radar data. *International Journal of Physical Sciences*, 5(12), 1890-1896.

1598 Mas, J. F., 1999. Monitoring land-cover changes: a comparison of change detection techniques.  
1599 *International Journal of Remote Sensing*, 20(1), 139-152.  
1600 <https://doi.org/10.1080/014311699213659>

1601 Mas, J. F., Flores, J. J., 2008. The application of artificial neural networks to the analysis of  
1602 remotely sensed data. *International Journal of Remote Sensing*, 29(3), 617-663.  
1603 <https://doi.org/10.1080/01431160701352154>

1604 Mason, D. C., Davenport, I. J., 1996. Accurate and efficient determination of the shoreline in  
1605 ERS-1 SAR images. *IEEE Transactions on Geoscience and Remote Sensing*, 34(5), 1243-1253.  
1606 <https://doi.org/10.1109/36.536540>

- 1607 Masria, A., Nadaoka, K., Negm, A., Iskander, M., 2015. Detection of shoreline and land cover  
1608 changes around Rosetta promontory, Egypt, based on remote sensing analysis. *Land*, 4(1), 216-  
1609 230. <https://doi.org/10.3390/land4010216>
- 1610 Mathers, S., Zalasiewicz, J., 1999. Holocene sedimentary architecture of the Red River delta,  
1611 Vietnam. *Journal of Coastal Research*, 314-325.
- 1612 Mazid, M. M., Ali, S., Tickle, K.S., 2010. Improved C4. 5 algorithm for rule based classification.  
1613 In *Proceedings of the 9th WSEAS international conference on Artificial intelligence, knowledge*  
1614 *engineering and data bases* (pp. 296-301). World Scientific and Engineering Academy and  
1615 Society (WSEAS).
- 1616 Motsholapheko, M. R., Kgathi, D. L., Vanderpost, C., 2011. Rural livelihoods and household  
1617 adaptation to extreme flooding in the Okavango Delta, Botswana. *Physics and Chemistry of the*  
1618 *Earth*, 36(14-15), 984–995. <https://doi.org/10.1016/j.pce.2011.08.004>
- 1619 Mouchot, M. C., Alföldi, T., De Lisle, D., McCullough, G., 1991. Monitoring the water bodies  
1620 of the Mackenzie Delta by remote sensing methods. *Arctic*, 21-28.  
1621 <https://doi.org/10.14430/arctic1566>
- 1622 Mukhopadhyay, A., Mukherjee, S., Mukherjee, S., Ghosh, S., Hazra, S., Mitra, D., 2012.  
1623 Automatic shoreline detection and future prediction: A case study on Puri Coast, Bay of Bengal,  
1624 India. *European Journal of Remote Sensing*, 45(1), 201-213.  
1625 <https://doi.org/10.5721/EuJRS20124519>
- 1626 Munasinghe, D., Cohen, S., Huang, Y. F., Tsang, Y. P., Zhang, J., Fang, Z., 2018.  
1627 Intercomparison of Satellite Remote Sensing-Based Flood Inundation Mapping Techniques.  
1628 *JAWRA Journal of the American Water Resources Association*, 54(4), 834-846.  
1629 <https://doi.org/10.1111/1752-1688.12626>
- 1630 Munasinghe, D.S.N., Cohen, S., Hand, B., (under review), A Review of Satellite Remote  
1631 Sensing Techniques of River Delta Morphology Change.
- 1632 Mustard, J. F., Sunshine, J. M., 1999. Spectral analysis for earth science: investigations using  
1633 remote sensing data. *Remote sensing for the earth sciences: Manual of remote sensing*, 3, 251-  
1634 307.
- 1635 Nandi, S., Ghosh, M., Kundu, A., Dutta, D., Baksi, M., 2016. Shoreline shifting and its  
1636 prediction using remote sensing and GIS techniques: a case study of Sagar Island, West Bengal  
1637 (India). *Journal of coastal conservation*, 20(1), 61-80. <https://doi.org/10.1007/s11852-015-0418-4>
- 1638 Nath, R. K., Deb, S. K., 2010. Water-body area extraction from high resolution satellite images-  
1639 an introduction, review, and comparison. *International Journal of Image Processing (IJIP)*, 3(6),  
1640 265-384.
- 1641 Niedermeier, A., Hoja, D., Lehner, S., 2005. Topography and morphodynamics in the German  
1642 Bight using SAR and optical remote sensing data. *Ocean Dynamics* 55(2), 100-109.  
1643 <https://doi.org/10.1007/s10236-005-0114-2>

1644 Niedermeier, A., Romaneessen, E., Lehner, S., 2000. Detection of coastlines in SAR images  
1645 using wavelet methods. *IEEE Transactions on Geoscience and Remote Sensing*, 38(5), 2270-  
1646 2281. <https://doi.org/10.1109/36.868884>

1647 Nienhuis, J.H., Törnqvist, T.E., Esposito, C.R., 2018. Crevasse splays versus avulsions: A recipe  
1648 for land building with levee breaches. *Geophysical Research Letters*, 45(9), 4058-4067.  
1649 <https://doi.org/10.1029/2018GL077933>

1650 Nitze, I., Grosse, G., 2016. Detection of landscape dynamics in the Arctic Lena Delta with  
1651 temporally dense Landsat time-series stacks. *Remote Sensing of Environment*, 181, 27-41.  
1652 <https://doi.org/10.1016/j.rse.2016.03.038>

1653 Niya, A.K., Alesheikh, A.A., Soltanpor, M., Kheirkhahzarkesh, M.M., 2013. Shoreline change  
1654 mapping using remote sensing and GIS. *International Journal of Remote Sensing Applications*,  
1655 3(3), 102-107.

1656 Orton, G. J., Reading, H.G., 1993. Variability of deltaic processes in terms of sediment supply,  
1657 with particular emphasis on grain size. *Sedimentology*, 40(3), 475-512.  
1658 <https://doi.org/10.1111/j.1365-3091.1993.tb01347.x>

1659 Ottinger, M., Kuenzer, C., Liu, G., Wang, S., Dech, S., 2013. Monitoring land cover dynamics in  
1660 the Yellow River Delta from 1995 to 2010 based on Landsat 5 TM. *Applied Geography*, 44, 53-  
1661 68. <https://doi.org/10.1016/j.apgeog.2013.07.003>

1662 Ozesmi, S.L., Bauer, M.E., 2002. Satellite remote sensing of wetlands. *Wetlands ecology and*  
1663 *management*, 10(5), 381-402. <https://doi.org/10.1023/A:1020908432489>

1664 Pal, M., Mather, P.M., 2003. An assessment of the effectiveness of decision tree methods for  
1665 land cover classification. *Remote sensing of Environment*, 86(4), 554-565.  
1666 [https://doi.org/10.1016/S0034-4257\(03\)00132-9](https://doi.org/10.1016/S0034-4257(03)00132-9)

1667 Pal, M., Mather, P.M., 2005. Support vector machines for classification in remote sensing.  
1668 *International Journal of Remote Sensing*, 26(5), 1007-1011.  
1669 <https://doi.org/10.1080/01431160512331314083>

1670 Paola, J.D., Schowengerdt, R.A., 1995. A review and analysis of backpropagation neural  
1671 networks for classification of remotely-sensed multi-spectral imagery. *International Journal of*  
1672 *Remote Sensing*, 16(16), 3033-3058. <https://doi.org/10.1080/01431169508954607>

1673 Passalacqua, P., 2017. The Delta Connectome: A network-based framework for studying  
1674 connectivity in river deltas. *Geomorphology*, 277, 50-62.  
1675 <https://doi.org/10.1016/j.geomorph.2016.04.001>

1676 Petropoulos, G.P., Kalivas, D.P., Griffiths, H.M., Dimou, P.P., 2015. Remote sensing and GIS  
1677 analysis for mapping spatio-temporal changes of erosion and deposition of two Mediterranean  
1678 river deltas: The case of the Axios and Aliakmonas rivers, Greece. *International Journal of*  
1679 *Applied Earth Observation and Geoinformation*, 35, 217-228.  
1680 <https://doi.org/10.1016/j.jag.2014.08.004>

1681 Postma, G., 1995. Sea-level-related architectural trends in coarse-grained delta complexes.  
1682 Sedimentary Geology, 98(1-4), 3-12. [https://doi.org/10.1016/0037-0738\(95\)00024-3](https://doi.org/10.1016/0037-0738(95)00024-3)

1683 Pu, H., Xia, W., Wang, B., Jiang, G.M., 2013. A fully constrained linear spectral unmixing  
1684 algorithm based on distance geometry. IEEE Transactions on Geoscience and Remote Sensing,  
1685 52(2), 1157-1176. <https://doi.org/10.1109/TGRS.2013.2248013>

1686 Ryu, J.H., Won, J.S., Min, K.D., 2002. Waterline extraction from Landsat TM data in a tidal flat:  
1687 a case study in Gomso Bay, Korea. Remote sensing of Environment, 83(3), 442-456.  
1688 [https://doi.org/10.1016/S0034-4257\(02\)00059-7](https://doi.org/10.1016/S0034-4257(02)00059-7)

1689 Sallam, R.L., Howson, C., Idoine, C.J., 2017. Augmented Analytics Is the Future of Data and  
1690 Analytics. <https://www.gartner.com/en/documents/3773164>

1691 Samarasinghe, S., 2016. Neural networks for applied sciences and engineering: from  
1692 fundamentals to complex pattern recognition. Auerbach publications.

1693 Sanchez-Arcilla, A., Jimenez, J.A., Valdemoro, H.I., 2012. The Ebro Delta: morphodynamics  
1694 and vulnerability. Journal of Coastal Research, 14(3).

1695 Sainju, A. M., Jiang, Z., 2017. Grid-based collocation mining algorithms on gpu for big spatial  
1696 event data: A summary of results. In International Symposium on Spatial and Temporal  
1697 Databases (pp. 263-280). Springer, Cham. [https://doi.org/10.1007/978-3-319-64367-0\\_14](https://doi.org/10.1007/978-3-319-64367-0_14)

1698 Seker, D.Z., Goksel, C., Kabdasli, S., Musaoglu, N., Kaya, S., 2003. Investigation of coastal  
1699 morphological changes due to river basin characteristics by means of remote sensing and GIS  
1700 techniques. Water Science and technology, 48(10), 135-142.  
1701 <https://doi.org/10.2166/wst.2003.0558>

1702 Seker, D.Z., Kaya, S., Musaoglu, N., Kabdasli, S., Yuasa, A., Duran, Z., 2005. Investigation of  
1703 meandering in Filyos River by means of satellite sensor data. Hydrological Processes: An  
1704 International Journal, 19(7), 1497-1508. <https://doi.org/10.1002/hyp.5593>

1705 Serra, P., Pons, X., Sauri, D., 2003. Post-classification change detection with data from different  
1706 sensors: Some accuracy considerations. International Journal of Remote Sensing, 24(16), 3311–  
1707 3340. <https://doi.org/10.1080/0143116021000021189>

1708 Seto, K.C., Woodcock, C.E., Song, C., Huang, X., Lu, J., Kaufmann, R.K., 2002. Monitoring  
1709 land-use change in the Pearl River Delta using Landsat TM. International Journal of Remote  
1710 Sensing, 23(10), 1985-2004. <https://doi.org/10.1080/01431160110075532>

1711 Sgavetti, M., Ferrari, C., 1988. The use of TM data for the study of a modern deltaic depositional  
1712 system. International Journal of Remote Sensing, 9(10-11), 1613-1627.  
1713 <https://doi.org/10.1080/01431168808954964>

1714 Sha, Z., Bai, Y., Xie, Y., Yu, M., Zhang, L., 2008. Using a hybrid fuzzy classifier (HFC) to map  
1715 typical grassland vegetation in Xilin River Basin, Inner Mongolia, China. International Journal  
1716 of Remote Sensing, 29(8), 2317-2337. <https://doi.org/10.1080/01431160701408436>

1717 Shalaby, A., Tateishi, R., 2007. Remote sensing and GIS for mapping and monitoring land cover  
1718 and land-use changes in the Northwestern coastal zone of Egypt. *Applied Geography*, 27(1), 28-  
1719 41. <https://doi.org/10.1016/j.apgeog.2006.09.004>

1720 Shen, F., Gao, A., Wu, J.P., Zhou, Y.X., Zhang, J., 2008. A remotely sensed approach on  
1721 waterline ex- traction of silty tidal flat for DEM construction, a case study in Jiuduansha Shoal of  
1722 Yangtze River. *Acta Geodaetica et Cartographica Sinica*, 37(1), 102–107.

1723 Shimabukuro, Y.E., Batista, G.T., Melio, E.M.K., Moreira, J.C., Duarte, V., 1998. Using shade  
1724 fraction image segmentation to evaluate deforestation in Landsat Thematic Mapper images of the  
1725 Amazon region. *International Journal of Remote Sensing*, 19(3), pp. 535–541.  
1726 <https://doi.org/10.1080/014311698216152>

1727 Singh, S., Talwar, R., 2013. Review on different change vector analysis algorithms based change  
1728 detection techniques. In: 2013 IEEE Second International Conference on Image Information  
1729 Processing (ICIIP-2013) (pp. 136-141). IEEE. <https://doi.org/10.1109/ICIIP.2013.6707570>

1730 Small, C., 2004. The Landsat ETM+ spectral mixing space. *Remote sensing of Environment*,  
1731 93(1-2), 1-17. <https://doi.org/10.1016/j.rse.2004.06.007>

1732 Steele, B.M., 2000. Combining multiple classifiers: an application using spatial and remotely  
1733 sensed information for land cover type mapping. *Remote Sensing of Environment*, 74(3), 545–  
1734 556. [https://doi.org/10.1016/S0034-4257\(00\)00145-0](https://doi.org/10.1016/S0034-4257(00)00145-0)

1735 Sun, N., Zhu, W., Cheng, Q., 2018. GF-1 and Landsat observed a 40-year wetland  
1736 spatiotemporal variation and its coupled environmental factors in Yangtze River estuary.  
1737 *Estuarine, Coastal and Shelf Science*, 207, 30-39. <https://doi.org/10.1016/j.ecss.2018.03.022>

1738 Suresh, M., Jain, K., 2018. Subpixel level mapping of remotely sensed image using colorimetry.  
1739 *The Egyptian Journal of Remote Sensing and Space Science*, 21(1), 65-72.  
1740 <https://doi.org/10.1016/j.ejrs.2017.02.004>

1741 Syvitski, J. P., Saito, Y., 2007. Morphodynamics of deltas under the influence of humans. *Global  
1742 and Planetary Change*, 57(3-4), 261-282. <https://doi.org/10.1016/j.gloplacha.2006.12.001>

1743 Syvitski, J. P., Kettner, A. J., Overeem, I., Hutton, E.W., Hannon, M.T., Brakenridge, G.R., Day,  
1744 J., Vörösmarty, C., Saito, Y., Giosan, L., Nicholls, R.J., 2009. Sinking deltas due to human  
1745 activities. *Nature Geoscience*, 2(10), 681. <https://doi.org/10.1038/ngeo629>

1746 Syvitski, J.P., Overeem, I., Brakenridge, G.R., Hannon, M., 2012. Floods, floodplains, delta  
1747 plains—a satellite imaging approach. *Sedimentary Geology*, 267, 1-14.  
1748 <https://doi.org/10.1016/j.sedgeo.2012.05.014>

1749 Tarboton, D.G., Idaszak, R., Horsburgh, J. S., Heard, J., Ames, D., Goodall, J.L., Merwade, V.,  
1750 Couch, A., Arrigo, J. and Hooper, R., 2014. HydroShare: advancing collaboration through  
1751 hydrologic data and model sharing.



1752 Thanh Noi, P., Kappas, M., 2018. Comparison of random forest, k-nearest neighbor, and support  
1753 vector machine classifiers for land cover classification using Sentinel-2 imagery. *Sensors*, 18(1),  
1754 18. <https://doi.org/10.3390/s18010018>

1755 Theseira, M.A., Thomas, G., Taylor, J.C., Gemmell, F., Varjo, J., 2003. Sensitivity of mixture  
1756 modelling to end-member selection. *International Journal of Remote Sensing*, 24(7), 1559-1575.  
1757 <https://doi.org/10.1080/01431160210146631>

1758 Tso, B., Mather, P.M., 2001. *Classification Methods for Remotely Sensed Data*, CRC Press.

1759 Ulrich, M., Grosse, G., Chabrilat, S., Schirrmeister, L., 2009. Spectral characterization of  
1760 periglacial surfaces and geomorphological units in the Arctic Lena Delta using field  
1761 spectrometry and remote sensing. *Remote Sensing of Environment*, 113(6), 1220-1235.  
1762 <https://doi.org/10.1016/j.rse.2009.02.009>

1763 Viaña-Borja, S. P., Ortega-Sánchez, M., 2019. Automatic Methodology to Detect the Coastline  
1764 from Landsat Images with a New Water Index Assessed on Three Different Spanish  
1765 Mediterranean Deltas. *Remote Sensing*, 11(18), 2186. <https://doi.org/10.3390/rs11182186>

1766 Walker, N. D., Hammack, A. B., 2000. Impacts of winter storms on circulation and sediment  
1767 transport: Atchafalaya-Vermilion Bay region, Louisiana, USA. *Journal of Coastal Research*, 996-  
1768 1010.

1769 Wang, F., Zhang, R., Zhao, H., Chen, X., 2019. Dynamic Evolution of the Yellow River Delta  
1770 coastline Based on Multi-Source Remote Sensing. *Ekoloji*, 28(107), 615-627.

1771 Warrender, C.E., Augusteihn, M.F., 1999. Fusion of image classification using Bayesian  
1772 techniques with Markov random fields. *International Journal of Remote Sensing*, 20(10), 1987-  
1773 2002. <https://doi.org/10.1080/014311699212308>

1774 Wei, W., Zhang, X., Chen, X., Tang, J., Jiang, M., 2008. Wetland mapping using subpixel  
1775 analysis and decision tree classification in the Yellow River delta area. *ISPRS Archives*, 38(B7),  
1776 667-670.

1777 White, K., El Asmar, H.M., 1999. Monitoring changing position of coastlines using Thematic  
1778 Mapper imagery, an example from the Nile Delta. *Geomorphology*, 29(1-2), 93-105.  
1779 [https://doi.org/10.1016/S0169-555X\(99\)00008-2](https://doi.org/10.1016/S0169-555X(99)00008-2)

1780 Wilson, P.A., 1997. Rule-based classification of water in Landsat MSS images using the  
1781 variance filter. *Photogrammetric Engineering & Remote Sensing*, 63(5), 485-491.

1782 Woodroffe, C.D., Nicholls, R.J., Saito, Y., Chen, Z., Goodbred, S.L., 2006. Landscape  
1783 variability and the response of Asian megadeltas to environmental change. In: Harvey, N. (Ed.),  
1784 *Global Change and Integrated Coastal Management*, 10, 277-314. Dordrecht, The Netherlands:  
1785 Springer. [https://doi.org/10.1007/1-4020-3628-0\\_10](https://doi.org/10.1007/1-4020-3628-0_10)

1786 Wu, C., 2009. Quantifying high-resolution impervious surfaces using spectral mixture analysis.  
1787 *International Journal of Remote Sensing*, 30(11), 2915-2932.  
1788 <https://doi.org/10.1080/01431160802558634>

- 1789 Xia, L., 1998. Measurement of rapid agricultural land loss in the Pearl River Delta with the  
1790 integration of remote sensing and GIS. *Environment and Planning B: Planning and Design*,  
1791 25(3), 447-461. <https://doi.org/10.1068/b250447>
- 1792 Xie, Y., Sha, Z., Yu, M., 2008. Remote sensing imagery in vegetation mapping: a review.  
1793 *Journal of Plant Ecology*, 1(1), 9-23. <https://doi.org/10.1093/jpe/rtm005>
- 1794 Xu, H. 2006. "Modification of Normalised Difference Water Index (NDWI) to Enhance Open  
1795 Water Features in Remotely Sensed Imagery." *International Journal of Remote Sensing* 27 (14):  
1796 3025–33. <https://doi.org/10.1080/01431160600589179>.
- 1797 Xu, J., Li, Z., Lei, L., Tian, B., Shan, Z., 2012. Land Cover Classification of Polarimetric SAR  
1798 Images for the Yellow River Delta Based on Support Vector Machine. In: 2012 International  
1799 Conference on Computer Vision in Remote Sensing (pp. 256-261). IEEE.  
1800 <https://doi.org/10.1109/CVRS.2012.6421271>
- 1801 Yang, X., 1996. Satellite Monitoring of the Dynamic Environmental Change of the Active  
1802 Yellow River Delta, China. *International Archives of Photogrammetry and Remote Sensing*, 31,  
1803 801-806.
- 1804 Yang, X., Damen, M.C.J., Van Zuidam, R.A., 1999. Satellite remote sensing and GIS for the  
1805 analysis of channel migration changes in the active Yellow River Delta, China. *International*  
1806 *Journal of Applied Earth Observation and Geoinformation*, 1(2), 146-157.  
1807 [https://doi.org/10.1016/S0303-2434\(99\)85007-7](https://doi.org/10.1016/S0303-2434(99)85007-7)
- 1808 Yates, M.L., Cozannet, G.L., 2012. Brief communication: Evaluating European Coastal  
1809 Evolution using Bayesian Networks. *Natural Hazards and Earth System Sciences*, 12(4), 1173-  
1810 1177. <https://doi.org/10.5194/nhess-12-1173-2012>
- 1811 Yeh, A.G.O., Li, X., 1997. An integrated remote sensing and GIS approach in the monitoring  
1812 and evaluation of rapid urban growth for sustainable development in the Pearl River Delta,  
1813 China. *International Planning Studies*, 2(2), 193-210.  
1814 <https://doi.org/10.1080/13563479708721678>
- 1815 Yoshino, K., Kawaguchi, S., Kanda, F., Kushida, K., Tsai, F., 2014. Very high resolution plant  
1816 community mapping at High Moor, Kushiro Wetland. *Photogrammetric Engineering & Remote*  
1817 *Sensing*, 80(9), 895-905. <https://doi.org/10.14358/PERS.80.9.895>
- 1818 Zhang, W., Xu, Y., Hoitink, A.J.F., Sassi, M.G., Zheng, J., Chen, X., Zhang, C., 2015.  
1819 Morphological change in the Pearl River Delta, China. *Marine Geology*, 363, 202-219.  
1820 <https://doi.org/10.1016/j.margeo.2015.02.012>
- 1821 Zhang, X., Treitz, P.M., Chen, D., Quan, C., Shi, L., Li, X., 2017. Mapping mangrove forests  
1822 using multi-tidal remotely-sensed data and a decision-tree-based procedure. *International Journal*  
1823 *of Applied Earth Observation And Geoinformation*, 62, 201-214.  
1824 <https://doi.org/10.1016/j.jag.2017.06.010>

- 1825 Zhang, X., Lu, Z., Jiang, S., Chi, W., Zhu, L., Wang, H., Lv, K., Wang, B., Yang, Z. (2018). The  
1826 progradation and retrogradation of two newborn Huanghe (Yellow River) Delta lobes and its  
1827 influencing factors. *Marine Geology*, 400, 38-48. <https://doi.org/10.1016/j.margeo.2018.03.006>
- 1828 Zhang, B., 2009. A CART Based Sub-pixel Method to Map Spatial and Temporal Patterns of  
1829 Prairie Pothole Lakes with Climatic Variability. Unpublished manuscript, Ohio State University,  
1830 Columbus, Ohio.
- 1831 Zhang, J., Foody, G.M., 1998. A fuzzy classification of sub-urban land cover from remotely  
1832 sensed imagery. *International Journal of Remote Sensing*, 19(14), 2721-2738.  
1833 <https://doi.org/10.1080/014311698214479>
- 1834 Zhao, B., Guo, H., Yan, Y., Wang, Q., Li, B., 2008. A simple waterline approach for tidelands  
1835 using multi-temporal satellite images: a case study in the Yangtze Delta. *Estuarine, Coastal and  
1836 Shelf Science*, 77(1), 134-142. <https://doi.org/10.1016/j.ecss.2007.09.022>
- 1837 Zhu, X., 2001. Remote sensing monitoring of coastline change in Pearl River Estuary. In: 22nd  
1838 Asian Conference on Remote Sensing (Vol. 5, p. 9).
- 1839 Zhu, C., Zhang, X., Huang, Q., 2018. Four decades of estuarine wetland changes in the Yellow  
1840 River delta based on Landsat observations between 1973 and 2013. *Water*, 10(7), 933.  
1841 <https://doi.org/10.3390/w10070933>